

# Wigner crystallization in a polarizable medium

G. Rastelli and S. Ciuchi

*Istituto Nazionale di Fisica della Materia and Dipartimento di Fisica  
Università dell'Aquila, via Vetoio, I-67010 Coppito-L'Aquila, Italy*

(Dated: November 20, 2018)

We present a variational study of the 2D and 3D Wigner crystal phase of large polarons. The method generalizes that introduced by S. Fratini, P. Quémerais [Mod. Phys. Lett. B **12** 1003 (1998)]. We take into account the Wigner crystal normal modes rather than a single mean frequency in the minimization procedure of the variational free energy. We calculate the renormalized modes of the crystal as well as the charge polarization correlation function and polaron radius. The solid phase boundaries are determined via a Lindemann criterion, suitably generalized to take into account the classical-to-quantum cross-over.

In the weak electron-phonon coupling limit, the Wigner crystal parameters are renormalized by the electron-phonon interaction leading to a stabilization of the solid phase for low polarizability of the medium. Conversely, at intermediate and strong coupling, the behavior of the system depends strongly on the polarizability of the medium.

For weakly polarizable media, a density crossover occurs inside the solid phase when the renormalized plasma frequency approaches the phonon frequency. At low density, we have a renormalized polaron Wigner crystal, while at higher densities the electron-phonon interaction is weakened irrespective of the *bare* electron-phonon coupling.

For strongly polarizable media, the system behaves as a Lorentz lattice of dipoles. The abrupt softening of the internal polaronic frequency predicted by Fratini and Quémérais is observed near the actual melting point only at very strong coupling, leading to a possible liquid polaronic phase for a wider range of parameters.

PACS numbers: 71.30.+h Metal-insulator transitions and other electronic transitions, 71.38.-k Polarons and electron-phonon interactions, 71.45.-d Collective effects

## INTRODUCTION

As it was first proposed by Wigner last century [1] the long range Coulomb interaction is able to stabilize a crystal of electrons, which eventually melts upon increasing the density at a quantum critical point. Experiments done on heterostructures [2] and quantum Monte Carlo simulations confirm this scenario [3, 4]. The presence of impurities is known to stabilize the crystal phase in two dimensions [5]. Another mechanism which could help the stabilization of the crystal phase is the effect of a polar material. As a single electron moves in a polar crystal, it polarizes its environment creating a new quasi-particle: a Fröhlich large polaron, with an enlarged effective mass [6, 7]. One expects then an enlargement of the Wigner crystal phase.

Interesting properties of the liquid phase in polar doped semiconductors arise also due to the interaction with the polarization, as for example, the mixing between plasmons and longitudinal optical (LO) phonons [8]. Such a mixing can be explained by assuming a long range interaction between the carriers and optical lattice vibrations of the Fröhlich type [9]. The resulting coupled LO-phonon-plasmon modes (CPPMs) are found in polar semiconductors (*n*-type GaP or *p*-type GaAs) [10]. Another interesting playground for this kind of physics is the surface-polaron, i.e. electron close to the surface of a polar crystal, which have been intensively studied especially for intermediate electron-phonon coupling  $\alpha$  as in

InSb where  $\alpha \sim 4.5$  [11] or in AgCl where  $\alpha \sim 3$  [12]. It has been also observed that the gate materials ( $\text{SiO}_2, \text{Al}_2\text{O}_3$  in organic thin films in field transistors are polar dielectrics and the interaction between the electrons and the surface phonons of the polar dielectric is relevant [13].

The aim of this work is to study the stabilization of the Wigner Crystal phase and its properties in the presence of a polarizable medium. We consider a general model in which the key feature is the presence of long range interaction which arise from direct Coulomb interactions between electrons and from the polarizable medium.

The presence of long range interactions, high polarizability and low carrier density is also a common feature of high-temperature superconductors. Of course, in these materials, short range interactions and lattice effects play an important role. Nonetheless, polarons have been detected by optical measurements in the antiferromagnetic insulating phase of both superconducting and parent cuprates [14, 15, 16]. Moreover, some evidence of strong electron-phonon coupling effects has been given recently in the underdoped regime [17]. A new interesting physics is introduced when studying these materials by the fact that the carrier concentration can be varied from very low to sufficiently high density. Prediction on optical properties and more specifically the behavior of the so called Mid Infrared Band (MIR) by varying the doping has been proposed according polaronic models [18, 19, 31] as well as its interpretation as charge ordering in stripes

[20]. A similar behavior has been also found in the optical properties of potassium doped Barium Bismutate[21].

When we consider a system composed of many interacting large polarons we are faced with the problem of screening of *both* electron-electron (e-e) and electron-phonon (e-ph) interactions as we increase the carrier density. A density crossover is therefore expected when the doping concentration is varied so that the plasma frequency approaches the optical longitudinal phonon frequency  $\omega_{LO}$ .

At high density, phonons cannot follow the much faster plasma oscillations of the electron gas and therefore they do not contribute to the screening of the e-e interactions. On the other hand, the electronic density fluctuations screen the e-ph interaction leading to the undressing of the electrons from their polarization clouds. As a consequence, the polaronic mass renormalization is hugely reduced [22]. In this case, the plasma frequency of the pure electron gas  $\omega_P^2 = 4\pi e^2 \rho / m$  is renormalized by the high frequency dielectric constant  $\varepsilon_\infty$

$$\omega_{P,H}^2 = \frac{\omega_P^2}{\varepsilon_\infty} \quad (1)$$

In the high density region, the self energy has been studied by a perturbative approach for weak e-ph coupling ( $m_{pol} \simeq m$ ) in the metallic phase[22]. The validity of this approach is ruled by the condition of  $\omega_{LO}^2 \ll \omega_P^2 / \varepsilon_\infty$ , since in this regime  $\omega_P^2 / \varepsilon_\infty$  is representative of electron density fluctuations. In this case, the electron screening weakens the *effective* e-ph coupling constant and it is argued that the perturbative approach is suitable also for semiconductors which have intermediate values of the *bare* e-ph coupling in the low doping phase. The same results have been obtained at weak and intermediate couplings by a ground state study [23]. An approach which is able to span the strong e-ph coupling regime has been presented in ref. [24], where an untrapping transition is found by increasing the density via the plasmon screening of the e-ph interaction. There it is concluded that there is no polaron formation at high density, irrespectively of the strength of the bare e-ph coupling constant.

At low density, the phonon energy scale (phonon-frequency) exceeds the electronic energy scale (plasma frequency). In this limit, the phonons can follow the oscillations of the slower electrons and they screen the e-e interaction. Thus, the frequency of the electron collective modes is renormalized by the static dielectric constant  $\varepsilon_0$ . Moreover, in the case of intermediate and strong e-ph coupling, polarons are formed [25] so that the appropriate expression for the general renormalized plasma frequency becomes

$$\omega_{P,L}^2 = \frac{m}{m_{pol}} \frac{\omega_P^2}{\varepsilon_0} \quad (2)$$

where  $m_{pol}$  is the polaron mass. In the case of *GaAs* the mass renormalization due to the e-ph interaction is

negligible, and usually eq.(2) is used to interpret the experimental data with  $m$ , the band mass of the carriers, in place of  $m_{pol}$  [10].

In ref.[26] an approximation is developed which allows to study a system of many interacting large polarons in the intermediate/low density regime for weak and intermediate coupling strengths. The phonon degrees of freedom are eliminated by a generalized Lee-Low-Pines transformation [27] obtaining an effective pair potential between electrons which is non-retarded, with a short range *attractive* term and a long range Coulomb repulsive term, statically screened by  $\varepsilon_0$ . The role of the inverse polarizability parameter  $\eta = \varepsilon_\infty / \varepsilon_0$  is evident in ref. [26]. In the case of  $\eta \ll 1$ , which is hereafter reported as the high polarizability regime, repulsive interaction and the retarded phonon-mediated attractive interaction are comparable leading to a softening of the energy of the collective modes at a finite value of the wave vector  $k$ , signaling a charge density wave instability. The attractive interaction term between the electrons plays a crucial role also at very low density where the ground state can be bi-polaronic below a certain value of the polarizability parameter [35], or can undergo a solid/liquid phase transition similar to the Wigner Crystallization (WC) [28]. In ref. [29, 30], a Large Polaron Crystal (LPC) is studied using a path-integral scheme. In ref [30], for  $\eta = 1/6$  (high polarizability regime), the authors conclude that in the weak and intermediate e-ph coupling regimes at  $T = 0$  the LPC melts toward a polaron liquid, but in the strong coupling regime a phonon instability appears near the melting. The authors argue this behavior from the softening of a long wavelength collective mode due to the e-e dipolar-interaction. A study which shows that the presence of long range order is not necessary for this kind of scenario has been presented in ref. [31] for a simplified model of a classical liquid of interacting dipoles, which are the polarons treated *à la* Feynman. The dipolar mode (internal frequency) is renormalized by the mean field of the other dipoles and it is shown to soften as the density increases, leading to the dissociation of the dipole (polaron).

The present work generalizes the approach of ref. [30] using a formalism which allows to span from high ( $\eta \ll 1$ ) to low polarizability regime ( $\eta \simeq 1$ ). We calculate the boundaries of the solid phase in three as well as in two dimensions. We also calculate, within the solid phase, the correlation function between the electron density and the charge polarization density. Our results confirm the relevant role of the parameter  $\eta$  in the strong e-ph coupling regime. According to the values of this parameter two distinct behaviors are found:

i) the high polarizability regime in which we found a scenario similar to that of ref. [30] i.e. the melting of the crystal is driven by the instability of the internal polaronic mode. Interestingly our more quantitative prediction push the instability-driven melting toward very

strong couplings leaving the possibility of a liquid polaronic phase for a wider range of parameters.

ii) the low polarizability regime, studied here even at strong coupling, in which we found that the undressing transition argued in the liquid phase [24] occurs also in the solid phase. Nonetheless e-ph interaction is able to stabilize the crystal against the liquid phase even for moderately polarizable mediums.

This paper is organized as follows: in the first section we illustrate the model and the approximations used, we introduce the quantities of interest, and we also discuss the Lindemann criterion used to determine the transition temperature. In the second section, we present the results in the three dimensional case. In the third section, the results of the two dimensional case are compared to the those in 3D. The conclusions are reported in the last section. Appendices contain technical details of the calculations.

## I - THE MODEL AND THE METHOD

### a) The model

The model describes a system of  $N$  interacting electrons in a  $D$ -dimensional space, which are coupled to longitudinal (undispersed) optical phonons. The Hamiltonian of the model is a generalization of that introduced by Fröhlich for a single large polaron [32] to  $N$ -large polarons [22]. We consider electrons as distinguishable particles. This approximation is justified inside the solid phase, where the overlap between the wavefunctions of different localized electrons is negligible [33]. Using the Path Integral technique [34] phonons can be easily traced out taking advantage of their gaussian nature and we end up with the following partition function [29]:

$$\mathcal{Z} = \oint \prod_i \mathcal{D}[\vec{r}_i(\tau)] e^{-\frac{1}{\hbar} \mathcal{S}_{eff}} \quad (3)$$

where  $\oint$  means the functional integration over all cyclic space-time paths of the particles  $\vec{r}_i(\tau)$  between zero and  $\beta = \hbar/k_B T$ . The effective electron action reads

$$\mathcal{S}_{eff} = \mathcal{S}_K + \mathcal{S}_{e-e} + \mathcal{S}_{e-ph-e}^{self} + \mathcal{S}_{e-ph-e}^{dist} + \mathcal{S}_J \quad (4)$$

where

$$\mathcal{S}_K = \int_0^\beta d\tau \sum_i \frac{1}{2} m |\dot{\vec{r}}_i(\tau)|^2 \quad (5)$$

$$\mathcal{S}_{e-e} = \frac{e^2}{2\varepsilon_\infty} \int_0^\beta d\tau \sum_{i \neq j} \frac{1}{|\vec{r}_i(\tau) - \vec{r}_j(\tau)|} \quad (6)$$

$$\mathcal{S}_{e-ph-e}^{self} = -\frac{\omega_{LO}(1-\eta)e^2}{4\varepsilon_\infty} \int_0^\beta d\tau \int_0^\beta d\sigma \sum_i \frac{D_o(\tau-\sigma)}{|\vec{r}_i(\tau) - \vec{r}_i(\sigma)|} \quad (7)$$

$$\mathcal{S}_{e-ph-e}^{dist} = -\frac{\omega_{LO}(1-\eta)e^2}{4\varepsilon_\infty} \int_0^\beta d\tau \int_0^\beta d\sigma \sum_{i \neq j} \frac{D_o(\tau-\sigma)}{|\vec{r}_i(\tau) - \vec{r}_j(\sigma)|} \quad (8)$$

$$\mathcal{S}_J = \beta \frac{(e\rho_J)^2}{2\varepsilon_0} V \int \frac{d\vec{r}}{r} - \int_0^\beta d\tau \sum_i \int d\vec{r} \frac{e^2 \rho_J / \varepsilon_0}{|\vec{r}_i(\tau) - \vec{r}|} \quad (9)$$

Here  $e^2$  is the electron charge,  $m$  is the electron band mass and  $V$  is the volume.  $(e\rho_J)$  is the static jellium charge density. The integration of phonons leads to the appearance of retarded e-e interaction terms -eqs.(7,8)-, where the phonon propagator is

$$D_o(\tau) = \frac{\cosh(\omega_{LO}[\beta/2 - \tau])}{\sinh(\beta\omega_{LO}/2)} \quad (10)$$

Using polaronic units (p.u.) ( $\hbar\omega_{LO}$  for energy,  $1/\omega_{LO}$  for imaginary time  $\tau$  and  $\sqrt{\hbar/m\omega_{LO}}$  for lengths)  $\mathcal{S}_{e-ph-e}$  becomes proportional to the dimensionless e-ph coupling constant  $\alpha$  defined as

$$\alpha = \frac{e^2}{\sqrt{2}} \frac{1-\eta}{\varepsilon_\infty} \sqrt{\frac{m}{\hbar^3 \omega_{LO}}} \quad (11)$$

while  $\mathcal{S}_{e-e}$  will be proportional to the e-e coupling constant

$$\alpha_e = \frac{\sqrt{2}e^2}{\varepsilon_\infty} \sqrt{\frac{m}{\hbar^3 \omega_{LO}}} \quad (12)$$

the ratio  $\alpha_e/\alpha = 2/(1-\eta)$  is thus solely determined by  $\eta = \varepsilon_\infty/\varepsilon_0$ : when  $\eta \simeq 1$  the Coulomb repulsion overwhelms the attraction mediated by phonons, while they become comparable for  $\eta \ll 1$ . Therefore, in the Fröhlich model, the inverse polarizability parameter rules the relative weight between the repulsive and attractive (phonon-mediated) interactions. This attraction can lead to a bipolaronic ground state as  $\alpha > \alpha_c(\eta)$  [35]. Roughly speaking this condition implies strong couplings  $\alpha > \alpha_c$  and high polarizability  $\eta < \eta_c$  where  $\alpha_c = 9.3$  and  $\eta_c = 0.131$  in 3D,  $\alpha_c = 4.5$  and  $\eta_c = 0.158$  in 2D case [35]. We have investigated the system for two values of  $\eta$ , representative respectively of the high and low polarizability regimes, and several values of the e-ph coupling  $\alpha$ . We choose respectively  $\eta = 1/6$  as in ref.[30], which gives  $\alpha_e/\alpha = 2.4$ , and  $\eta = 0.90519$  so that the coupling  $\alpha_e/\alpha$  is increased by a factor of ten [36]. For these values of  $\eta$ , no bipolaron ground state exists.

### b) The harmonic variational approximation in the solid phase

We generalize the harmonic variational approach originally introduced in ref.[29] to study the model eq.(4). First of all we recall here the variational theory in the path integral formalism. Let us consider a suitable trial action  $\mathcal{S}_T$  which depends on some variational parameters. Substituting  $\mathcal{S}_{eff}$  with  $\mathcal{S}_T$  in eq.(3) we obtain the partition function  $\mathcal{Z}_T$  for the trial action and the free energy associated to it  $\mathcal{F}_T = -k_B T \ln \mathcal{Z}_T$ . Then the exact free energy can be expressed as

$$\mathcal{F} = \mathcal{F}_T - k_B T \ln \left\langle e^{-\frac{1}{\hbar} \Delta \mathcal{S}} \right\rangle_T \quad (13)$$

where  $\Delta \mathcal{S} = \mathcal{S}_{eff} - \mathcal{S}_T$  and the mean value  $\langle \dots \rangle_T$  is

$$\langle \dots \rangle_T = \frac{1}{\mathcal{Z}_T} \oint \prod_i \mathcal{D}[\vec{r}_i(\tau)] (\dots) e^{-\frac{1}{\hbar} \mathcal{S}_T} \quad (14)$$

The variational free energy is obtained by a cumulant expansion of the logarithm appearing in eq. (13). At first order in  $\Delta \mathcal{S}$  it reads:

$$\mathcal{F}_V = \mathcal{F}_T + \frac{1}{\beta} \langle \Delta \mathcal{S} \rangle_T \quad (15)$$

where  $\mathcal{F}_V \geq \mathcal{F}$ . To define a suitable trial action we proceed in two steps as in ref.[29]. First we treat the self interaction term  $\mathcal{S}_{e-ph-e}^{self}$  of eq. (7) *a la Feynman* [37, 38]. Therefore we substitute  $\mathcal{S}_{e-ph-e}^{self}$  with  $\mathcal{S}_{Feyn}$

$$\mathcal{S}_{Feyn} = \frac{(v^2 - w^2)mw}{8} \sum_i \int_0^\beta d\tau \int_0^\beta d\sigma D_V(\tau - \sigma) |\vec{r}_i(\tau) - \vec{r}_i(\sigma)|^2 \quad (16)$$

$v$  and  $w$  are the two variational parameters. The variational propagator  $D_V(\tau)$  is given by eq. (10) with  $w$  replacing  $\omega_{LO}$ . We remind that  $\mathcal{S}_{Feyn}$  eq.(16) can be obtained by integrating out an action where each electron interacts elastically ( $K_T = m(v^2 - w^2)$ ) with a fictitious particle of mass  $M_T = m[(v^2/w^2) - 1]$ . Then  $v$  is the internal frequency and  $1/\mu = 1/m + 1/M_T$  is the reduced mass of the two particle system

As a second step, we treat the  $\mathcal{S}_{e-e}$ ,  $\mathcal{S}_J$  eqs.(6,9) and the distinct part ( $\mathcal{S}_{e-ph-e}^{dist}$ ) eq.(8) of  $\mathcal{S}_{eff}$  in eq.(4) by means of a harmonic approximation. Expressing the position of the electrons around the Wigner lattice points as  $\vec{r}_i = \vec{u}_i + \vec{X}_i$  where  $\vec{X}_i$  are the vectors of the Bravais lattice (b.c.c. in 3D, hexagonal in 2D) and omitting the constant terms of the solid phase potential energy, we obtain the following harmonic variational action:

$$\mathcal{S}_T = \mathcal{S}_K + \mathcal{S}_{Feyn} + \mathcal{S}_J^H + \mathcal{S}_{e-e}^H + \mathcal{S}_{e-ph-e}^{H,dist} \quad (17)$$

where

$$\mathcal{S}_K = \int_0^\beta d\tau \sum_i \frac{1}{2} m |\dot{\vec{u}}_i(\tau)|^2 \quad (18)$$

$$\begin{aligned} \mathcal{S}_{e-J}^H + \mathcal{S}_{e-e}^H &= \int_0^\beta d\tau \sum_i \frac{1}{2} m \frac{\omega_W^2}{\varepsilon_0} |\vec{u}_i(\tau)|^2 \\ &+ \int_0^\beta d\tau \frac{e^2}{2\varepsilon_\infty} \sum_{i \neq j} \vec{u}_i(\tau) \overline{\mathcal{I}}_{ij} \vec{u}_j(\tau) \end{aligned} \quad (19)$$

$$\mathcal{S}_{e-ph-e}^{H,dist} = -\frac{\omega_{LO} e^2}{4\bar{\varepsilon}} \sum_{i \neq j} \int_0^\beta d\tau \int_0^\beta d\sigma D_o(\tau - \sigma) \vec{u}_j(\sigma) \overline{\mathcal{I}}_{ij} \vec{u}_i(\tau) \quad (20)$$

In eq.(19), the Wigner frequency is defined as usual in 3D as  $\omega_{W,3D}^2 = \omega_P^2/3$  (for the 2D case see eq.(72) in Appendix B). The force constants  $[\overline{\mathcal{I}}_{ij}]_{\alpha\beta}$  are obtained through a harmonic expansion for the Coulomb potential (see appendix B). In our calculations, we neglect the anharmonic terms in  $\Delta \mathcal{S}$  of eq. (15), therefore we get

$$\mathcal{F}_V = \mathcal{F}_T + \frac{1}{\beta} \langle \mathcal{S}_{e-ph-e}^{self} - \mathcal{S}_{Feyn} \rangle_T \quad (21)$$

We have minimized  $\mathcal{F}_V/N$  varying  $w, v$  at given density and temperature keeping  $\alpha$  and  $\eta$  fixed. Minimization is constrained by a convergence condition on the gaussian integrals appearing in  $\mathcal{F}_V$ . The constrained minimization procedure is described in appendix C.

So far, the discussed scheme appears very similar to the one of ref.[29]. However, we stress that the  $\mathcal{F}_V$ , which we have minimized to obtain the variational parameter  $v$  and  $w$ , contains the hetero-interaction terms  $\mathcal{S}_{e-e}^H$  and  $\mathcal{S}_{e-ph-e}^{H,dist}$ , which are not included in the minimization procedure of ref. [29]. Moreover, we have also used the *whole* trial action  $\mathcal{S}_T$  eq.(17) to calculate the mean electronic fluctuation which we have used in the Lindemann rule, as explained in the following section.

### c) Lindemann rule and phase diagrams

To determine the solid-liquid transition we use the phenomenological Lindemann criterion, suitably generalized to take into account the classical-to-quantum cross-over [39]:

$$\frac{\langle |\vec{u}|^2 \rangle_{eff}}{d_{n.n.}^2} = \gamma^2 (\eta_q) \quad (22)$$

in the l.h.s. of eq. (22) we have the Lindemann ratio between the mean fluctuation of the electrons around its equilibrium position and the nearest neighbors distance  $d_{n.n.}$ . When it exceeds a critical value (r.h.s. of eq. (22)), the solid melts. In eq.(22)  $\langle \dots \rangle_{eff}$  is the average taken

over  $\mathcal{S}_{eff}$  eq.(4). The average is carried out at the zeroth order in the cumulant expansion as an average over  $\mathcal{S}_T$  eq.(17).

Contrary to the classical liquid-solid transition, where the Lindemann rule predicts the full melting line using a constant  $\gamma = \gamma_{cl}$ , in the case of a quantum crystal an interpolating formula for  $\gamma$  is necessary to determine the melting line as obtained by comparing the free-energies of the two phases calculated using quantum simulations [3]. Hence the analytic expansion of the quantum corrections to the classical free energy respect to the quantum parameter  $\eta_q$  and the zero-temperature melting density provides the interpolating function (r.h.s. of eq.22) for  $\gamma(\eta_q)$  [39].  $\eta_q$  is defined for the pure electron gas as the ratio between zero point and thermal activation energies as:

$$\eta_q = \frac{\hbar\omega_p}{2k_B T}. \quad (23)$$

We have chosen for the function  $\gamma(\eta_q)$  the form of refs. [40, 41]:

$$\gamma(T, r_s) = \gamma_q - \frac{\gamma_q - \gamma_{cl}}{1 + A\eta_q^2} \quad (24)$$

Formula (24) has a single interpolation parameter  $A$  which we take as  $A = 1.62 \cdot 10^{-2}$  in 3D [40] and  $A = 3 \cdot 10^{-2}$  in 2D [41].

The chosen value of  $\gamma_{cl} = 0.155$  is such that the classical transition lines ( $T = 2/\Gamma_c r_s$  a.u.) are recovered in both the 3D ( $\Gamma_c = 172$  from ref. [40]) and 2D ( $\Gamma_c = 135$  from ref. [41]) cases. The value  $\gamma_q = 0.28$  is chosen to reproduce the zero temperature quantum transition in 3D ( $r_s = 100$  a.u. from ref. [40]) and 2D ( $r_s = 37$  a.u. from ref. [41]).

Roughly speaking, the transition curve is limited by the classical line  $T = (2/\Gamma_c) 1/r_s$  and the quantum melting  $1/r_s = 1/r^c$ . The actual transition curve is a smooth interpolation between these two limiting behaviors. Of course, the precise knowledge of the interpolation formula (i.e. the knowledge of parameters appearing in it) is critical only for the determination of the transition line at high temperatures (see fig.1).

We notice that the particular values of the parameters entering in eq.(24) depend on the kind of statistics (boson, fermion) and on the system parameters only via the ratio  $\eta_q$  [42]. This parameter depends on the mass of the particles via  $\omega_p$ , which measures the zero point energy of the oscillator which eventually melts [43]. Therefore, to generalize the Lindemann criterion to the interacting large polaron system we are left with the alternative of choosing between the electron and the polaron effective mass in eqs. (23,24).

The polaron exists as a well defined quasiparticle when both  $k_B T \ll \hbar\omega_{LO}$  [44] and  $\hbar\bar{\omega}_P \ll \hbar\omega_{LO}$ . The second condition relies on the effectiveness of the e-ph interaction, as explained in the introduction. Therefore, if both

conditions are fulfilled, we have to replace  $\omega_P$  in eq. (23) by  $\bar{\omega}_P$  given by eq. (2). In this case, between the classical ( $\eta_q \simeq 0$ ) and quantum melting ( $\eta_q \rightarrow \infty$ ), we have a polaronic Wigner Crystal. This is the case of the high polarizability ( $\eta = 0.17$ ).

For low polarizability ( $\eta = 0.9$ ), a cross-over occurs inside the solid phase when  $\hbar\bar{\omega}_P \sim \hbar\omega_{LO}$  and the coupling is intermediate or strong, as it will be discussed in details later on. In this case, we still have a classical melting of polaronic quasi-particles, but the quantum melting involves the undressed electrons. In the classical regime (low density), the transition line does not depend appreciably on the quantum parameter, as  $\gamma$  attains its classical limit ( $\eta_q \rightarrow 0$ ). In the quantum regime at high density and low temperatures ( $\eta_q \rightarrow \infty$ ) the function  $\gamma$  eq. (24) saturates to its quantum value  $\gamma_q$  and the density  $r_c$  of the quantum melting does not depend of the choice for the quantum parameter  $\eta_q$ . Instead, a pronounced dependency on the actual value of the quantum parameter is expected in the calculation of the melting line at high temperatures and intermediate densities.

For  $\eta = 0.9$  we choose the high density estimate  $\omega_P/\sqrt{\epsilon_\infty}$  as the plasma frequency entering in eq. (23). This choice produces, in the intermediate temperature/density region, an upward deviation (fig. 1 lower panel) from the classical slope. This is a drawback of our approximation, which is however correct at low temperatures for both low and high density.

We finally discuss to which extent we use the Lindemann criterion in 2D, and more generally on the applicability of the harmonic theory in 2D. This is related to the well known problem of the existence of two dimensional crystalline long-range order at finite temperature [45]. In a pure electron gas, for  $T = 0$ , this problem does not arise and the properties of the system in the harmonic approximation have been studied extensively [46, 47]. The general statement for the classical impossibility of 2D crystalline long-range order was first pointed out by Peierls [48]. Landau [49] gave a general argument according to which fluctuations destroy crystalline order possessing only a one or two dimensional periodicity. The first microscopic treatment of the problem (not valid in case of Coulomb interaction) is due to Mermin [45]: his proof is based on Bogolyubov's inequality that leads to the conclusions that the Fourier component of the mean density is zero for every vector  $k$  in the thermodynamic limit. Motivated by the interest of the 2D electron gas, Mermin's proof was critically re-examined for the long range potential [50, 51]. We discuss here the argument of Peierls for the 2D electron crystal. The mean square thermal fluctuations of a generic classical particle diverges in two dimensions for an infinite harmonic crystal. At low density, we have  $\eta_q \simeq 0$  and the mean electronic fluctuation can be approximated by the

classical value

$$\langle u^2 \rangle_{CI,WC} = \frac{Dk_B T}{2m\omega_P^2} \mathcal{M}_{-2} \quad (25)$$

$$\mathcal{M}_{-2} = \int d\omega \rho(\omega) \frac{\omega_P^2}{\omega^2} \quad (26)$$

where  $\mathcal{M}_{-2}$  is the dimensionless second inverse moment of the density of the states (DOS) of charge fluctuation normal modes in the pure WC ( $\rho(\omega)$ ). Since long-wavelength acoustical vibrational modes scale as  $\omega = c_s k$ , the DOS is given at low energies by  $\rho(\omega) \sim \omega$  for  $\omega \rightarrow 0$  [52] and the integral eq.(25) diverges logarithmically. However, a lower cut-off in the frequency spectrum, which exists for a large but finite system studied in laboratory [52] or in a computer simulation [4, 53], removes the logarithmic divergence. We have chosen a cut-off frequency which corresponds to a fixed number of particles  $N \simeq 5 \cdot 10^5$ . The dependence of the cut-off is discussed in appendix A. There and later on it is shown that our results are cut-off independent for low temperatures and density near the quantum critical point. Therefore we will discuss 2D case only in this region.

#### d) Correlation functions and polaron radius

We now introduce the correlation functions between the electron and the polarization densities for a system with N electrons, and a measure of the polaron radius.

The polarization density vector of the medium is associated to the optical phonon modes  $Q_{\vec{q}}$  through the relation [7]:

$$\vec{P}(\vec{r}) = \sum_{\vec{k}} i \frac{\omega_{LO}}{\sqrt{4\pi\epsilon V}} \frac{\vec{k}}{|\vec{k}|} e^{i\vec{k}\vec{r}} Q_{\vec{k}}. \quad (27)$$

The induced charge density is defined by [7]

$$n_i(\vec{r}) = -\frac{1}{e} \vec{\nabla} \cdot \vec{P}(\vec{r}) \quad (28)$$

Correlation between a given electron and the induced charge density can be defined as:

$$C_1(\vec{r}^{\vec{j}}, \vec{r}) = \frac{\langle \rho_1(\vec{r}) n_i(\vec{r}^{\vec{j}}) \rangle}{\langle \rho_1(\vec{r}) \rangle} \quad (29)$$

with  $\rho_1(\vec{r}) = \delta(\vec{r} - \vec{r}_1)$ . In eq.(29) we have chosen the appropriate normalization for the correlation function between one electron and the polarization. Integrating out the phonons we arrive at the following expression, in which we express all quantities in terms of averages weighted by the effective action eqs.(4)

$$C_1(\vec{r}^{\vec{j}}, \vec{r}) = \frac{1}{\epsilon} \int_0^\beta d\tau \frac{\omega_{LO}}{2} D_o(\tau) \frac{\langle \rho_1(\vec{r}) \rho(\vec{r}^{\vec{j}}, \tau) \rangle_{eff}}{\langle \rho_1(\vec{r}) \rangle_{eff}} \quad (30)$$

In eq.(30)  $\rho(\vec{r}^{\vec{j}}, \tau)$  is the path density defined by:

$$\rho(\vec{r}^{\vec{j}}, \tau) = \delta(\vec{r}^{\vec{j}} - \vec{r}_1(\tau)) + \sum_{i \neq 1} \delta(\vec{r}^{\vec{j}} - \vec{r}_i(\tau)) \quad (31)$$

where we have explicitly separated the contribution  $\rho_1(\vec{r}^{\vec{j}}, \tau)$  due to the electron 1 from the remainder. The first contribution in r.h.s. of eq. (31) give rise to a self term in the correlation function eq. (30) given by

$$C_1^{self} = \frac{1}{\epsilon} \int_0^\beta d\tau \frac{\omega_{LO}}{2} D_o(\tau) \frac{\langle \rho_1(\vec{r}) \rho_1(\vec{r}^{\vec{j}}, \tau) \rangle_{eff}}{\langle \rho_1(\vec{r}) \rangle_{eff}} \quad (32)$$

Notice that in the limit of a single isolated polaron, this correlation function reduces to the one evaluated in ref. [44]. Assuming an electron at origin ( $\vec{r} = 0$ ), we have  $C_1^{self}$  depending only on  $\vec{r}^{\vec{j}}$ . The radial induced charge density  $g(r)$  can be defined as

$$g(r) = r^{D-1} \int d^D \Omega C_1^{self}(\vec{r}) \quad (33)$$

Using this function, we can define, as a measure of the polaronic radius, the square root of the second moment of  $g(r)$

$$R_p = \left( \int_0^\infty dr r^2 g(r) \right)^{1/2} \quad (34)$$

The actual calculation for the mean values appearing in eq.(32) are carried out at the zeroth order of the variational cumulant expansion. Explicit calculations are reported in Appendix E.

## II - RESULTS IN 3D

Here we compare the low ( $\eta = 0.9$ ) and high ( $\eta = 1/6$ ) polarizability cases in 3D. For each polarizability, the electron-phonon coupling constant  $\alpha$  spans from weak to strong coupling regime:  $\alpha = 1, 3, 5, 7, 9, 11, 13, 15$ . Phase diagrams obtained through the Lindemann criterion are shown in figs. 1 where the solid-liquid transition lines of the LPC are compared to that of the pure Wigner crystal. Density is expressed in term of the adimensional parameter  $r_s^3 = a_o^3 / [(4\pi/3)\rho]$ , where  $a_o$  is the Bohr radius with ( $m = m_e, \epsilon_\infty = 1$ ). A common feature of both the low and high polarizability cases is the enlargement *in density scale* of the solid phase as far as e-ph coupling increases. However, in both cases, the solid phase cannot be stabilized for any density by increasing the e-ph interaction, and the quantum melting point saturates at a maximum value when the e-ph coupling is very strong. To illustrate this different behavior it is worth to introduce a simplified model.

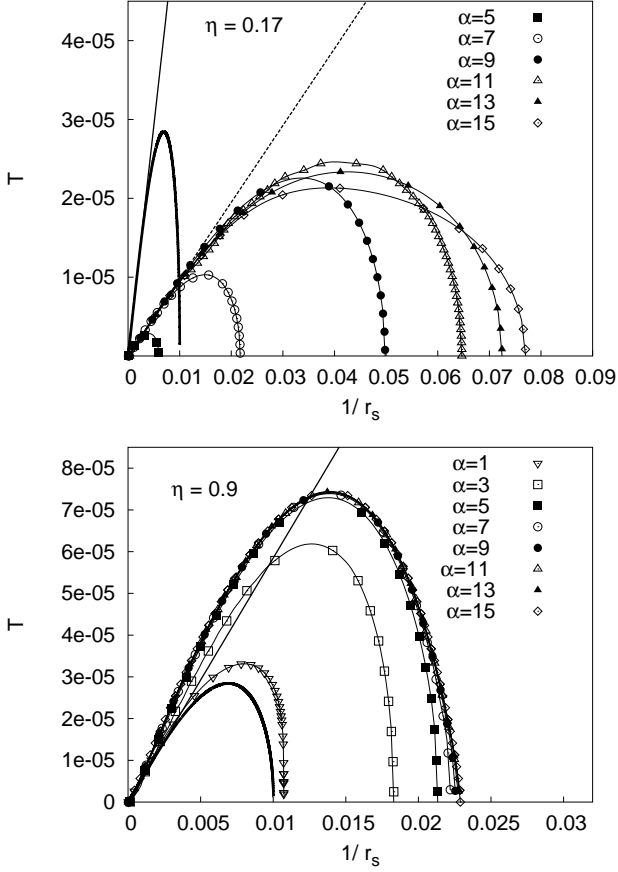


FIG. 1: Phase diagrams for a 3D LPC for  $\eta = 0.17$  (upper panel) and  $\eta = 0.9$  (lower panel). Atomic units (a.u.) are used for temperature and  $r_s$  (see text). Solid phase is enclosed below transition lines. In both the upper and the lower panels continuous bold curve is the pure WC transition line and solid line gives the classical melting. In the upper panel dashed line is the renormalized classical melting.

### a) A simplified model

In the simplified model, introduced in ref. [30], the electrons interact with each other and with *all* the fictitious particles ( $\{\vec{R}_i\}$ ) with mass  $M_T$  which represent the polarization of the medium. After integration of the fictitious particles, we obtain the effective electronic lagrangian  $\mathcal{L}_{eq}$ . The effective harmonic lagrangian  $\mathcal{L}_{eq}$  generated by the simplified model corresponds exactly to the lagrangian of the action  $\mathcal{S}_T$  eq.(17) with the parameter  $w = \omega_{LO}$ . This approximation restricts the space of variational parameters, and therefore gives rise to a worse estimate for the free energy. Nonetheless, it allows to describe the physics of the system in a simplified fashion.

Each WC's branch is splitted in two branches for the LPC and the frequencies of the system are given by the two roots  $\Omega_{\pm}^2(\omega_{s,\vec{k}})$  (eqs.(24,25) of the work [30]), where  $\omega_{s,\vec{k}}$  are the WC frequencies with wave vector  $\vec{k}$  and

branch index  $s$ . The expression for the mean fluctuation  $\langle u^2 \rangle_{eq}$  of electrons around their equilibrium value in the simplified model is easily obtained by inserting  $w = \omega_{LO}$  in the variational expression  $\langle u^2 \rangle_T$  (see Appendix D, eqs.100,101,102). The  $\Omega_{\pm}$  branches give rise to a natural splitting of contributions to the fluctuation

$$\frac{\langle u^2 \rangle_{eq}}{d_{n.n.}^2} = \frac{\langle u^2 \rangle_+}{d_{n.n.}^2} + \frac{\langle u^2 \rangle_-}{d_{n.n.}^2} \quad (35)$$

In the low density regime of the simplified model [30], i.e. when phonons are much faster than density fluctuations, the spectrum can be decomposed into the renormalized WC frequencies  $\tilde{\Omega}_-(\omega_{s,\vec{k}})$  and the polaronic optical frequencies  $\tilde{\Omega}_+(\omega_{s,\vec{k}})$ , which can be obtained by expanding the general solutions  $\Omega_{\pm}^2(\omega_{s,\vec{k}})$  with respect to the parameter  $\epsilon_{s,\vec{k}}$  defined as

$$\epsilon_{s,\vec{k}} = \omega_{s,\vec{k}}^2 / (\epsilon_0 v^2) \quad (36)$$

which is small for *all* frequencies  $\omega_{k,s}$  of WC normal modes at low density regime.

The first part of the spectrum represents the *low* frequencies associated to the oscillation of the center of mass ( $m_{pol} = m + M_T$ ) of the two-particle system, i.e. the electron and its relative fictitious particle (polarization), while the second part of the spectrum describes the dipolar modes associated to the internal motion of oscillating electron-fictitious particle system (fig.1 of ref.[30]). Dipolar modes are weakly dispersed around the frequency  $\omega_{pol}$  (eq.(25) of ref.[30]) defined as the  $k = 0$  mode of the polaronic branches. It represents the internal frequency of oscillation of the electron inside its polarization well.

### b) Classical and renormalized quantum melting

Now let us consider the classical transition. This transition is located in the low density regime of the simplified model. Using the low density expansion for the spectrum ( $\tilde{\Omega}_-(\omega_{s,\vec{k}}), \tilde{\Omega}_+(\omega_{s,\vec{k}})$ ), it is possible to associate each term,  $\langle u^2 \rangle_+$  and  $\langle u^2 \rangle_-$ , to a definite degree of freedom of the two-particle system, i.e. to the fluctuation of the center of mass

$$\langle u^2 \rangle_- \simeq \int d\omega \rho(\omega) \frac{\hbar D \coth \left[ \hbar \left( \sqrt{\frac{m}{\epsilon_0 m_{pol}}} \right) \omega / 2k_B T \right]}{2 m_{pol} \left( \sqrt{\frac{m}{\epsilon_0 m_{pol}}} \right) \omega} \quad (37)$$

and to the fluctuation associated to the internal dipolar mode with  $\vec{\rho} = \vec{u} - \vec{R}_T$  and reduced mass  $\mu$

$$\langle u^2 \rangle_+ \simeq \left( \frac{M_T}{m + M_T} \right)^2 \frac{\hbar D}{2\mu\omega_{pol}} \coth \left( \frac{\hbar\omega_{pol}}{2k_B T} \right) \quad (38)$$

In this case we can easily estimate the ratio between electronic fluctuations in LPC and in WC by taking into account only the renormalized WC spectrum, i.e. the fluctuation associated to the center of mass eq.(37). Using eq.(25) we have  $\langle u^2 \rangle_{LPC} / \langle u^2 \rangle_{WC} = 1/\epsilon_0$  then by Lindemann criterion eq. (22) and by eq. (25) at a given density, the critical temperature ratio also equals  $1/\epsilon_0$

$$\frac{T_{LPC}^{Cl}}{T_{WC}^{Cl}} = \frac{1}{\epsilon_0}. \quad (39)$$

Therefore, the slope of the classical transition line is lowered by the same factor, as can be seen in fig. 1 (upper panel), where  $\epsilon_0$  is appreciably large.

The quantum melting is ruled by the zero point fluctuations of the electronic oscillations. A zero temperature estimate for the pure WC gives

$$\langle u^2 \rangle_{WC} = \frac{\hbar D}{2m\omega_P} \mathcal{M}_{-1} \quad (40)$$

$$\mathcal{M}_{-1} = \int d\omega \rho(\omega) \frac{\omega_P}{\omega} \quad (41)$$

where  $\mathcal{M}_{-1}$  is the dimensionless inverse moment of the WC DOS. If we consider only the renormalized WC spectrum eq.(37), and we take into account eq.(40), we get for the LPC

$$\frac{\langle u^2 \rangle_{Q,LPC}}{\langle u^2 \rangle_{Q,WC}} = \left( \frac{m\epsilon_0}{m_{pol}} \right)^{1/2} \left( \frac{r_s}{r_s(WC)} \right)^{3/2}. \quad (42)$$

then using Lindemann criterion we obtain at the quantum critical point ( $r_s = r_c$ )

$$\frac{r_c(WC)}{r_c} = \frac{m_{pol}}{m\epsilon_0}. \quad (43)$$

eq.(43) generalizes the result of the ref.[29] where the Lindemann rule was discussed within a mean field approach.

At high polarizability  $\langle u^2 \rangle_-$  eq.(37) is the leading term in the mean electronic fluctuation  $\langle u^2 \rangle_{eq}$  eq.(35) near the quantum melting for small and intermediate couplings  $\alpha \leq 7$ . In this case, the quantum melting density scales as eq.(43). Notice that at weak coupling the mass renormalization is weak, but phonon screening through  $\epsilon_0$  dominates, leading to quantum melting at lower densities than in a purely electronic Wigner Crystal (upper panel figs.1,2). At low polarizability eq.(43) is valid up to  $\alpha \simeq 3$  (fig.2).

Upon increasing the coupling,  $m_{pol}$  scales as  $\sim \alpha^4$  in strong coupling and eq.(43) predicts a divergence of the quantum melting density. As shown in figs. 1,2, the quantum melting density saturates to an  $\alpha$ -independent value at strong coupling, and the prediction of eq. (43) is no longer valid. We will see in the next subsection that deviation from the prediction of eq. (43) arise from different reasons in low and high polarizability cases.

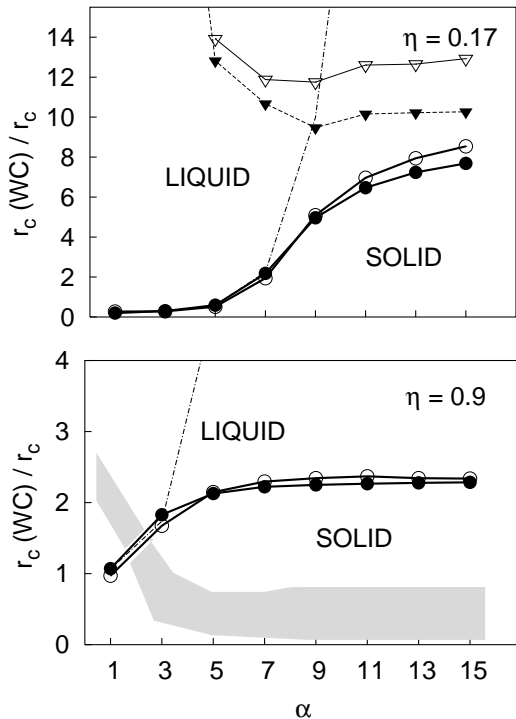


FIG. 2: Zero temperature phase diagram in the 2D (open symbols) and 3D (solid symbols) cases. In 2D  $\alpha$  has been scaled according the zero density limit. Circles are the scaled quantum melting  $r_c$  vs e-ph coupling constant  $\alpha$ . Dashed line is the renormalized quantum melting transition curve from eq.(43). Upper panel:  $\eta = 0.17$ . Triangles locates the softening of  $\omega_{pol}$ . Lower panel:  $\eta = 0.9$ . The shaded area encloses the cross-over region inside the solid phase.

### c) High polarizability: softening of internal mode

This is the case in which the polarization gives a large contribution to the total interaction energy of the system. The system can be thought as being composed by interacting dipoles which are made by electrons surrounded by their polarization.

In the case of strong e-ph coupling we observe a saturation of the critical quantum melting density. In fig. 3 the electronic fluctuation is reported for  $\alpha = 13$ . Contrary to the small/intermediate coupling case,  $\langle u^2 \rangle_+$  eq.(38) is now the leading term near the quantum melting. The melting density given by eq.(43) is not a good estimate due to the contribution of polaronic optical modes which is now important at the quantum melting. The same scenario of ref.[30] is recovered: the optical polaronic frequencies drive the melting at strong coupling and high polarizability. Moreover we notice that  $\langle u^2 \rangle_+ \sim (1/\omega_{pol})$  and, as density approaches a critical value,  $\omega_{pol}$  softens inducing an abrupt increase of electron fluctuation which is dominated by the term  $\langle u^2 \rangle_+$  (see fig.3). Same behav-



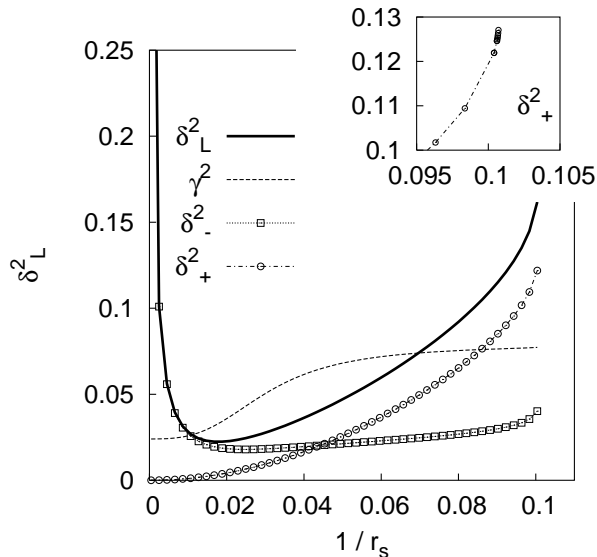


FIG. 3: The Lindemann ratio (solid line) and the function  $\gamma$  (dashed line) for  $\eta = 0.17$  and  $\alpha = 13$ ,  $T = 1.10^{-5}$  (a.u.). Contributions  $\delta_{\pm}^2 = \langle u^2 \rangle_{\pm} / d_{n,n}^2$  of the simplified model eq.(35) are also shown. The inset shows the abrupt slope increase of the term  $\delta_{+}^2$ .

ior for  $\omega_{pol}$  is reported in ref.[30] and explained in term of the attractive interaction between the polarons (polarization catastrophe). We stress however that employing a more quantitative Lindemann criterion together with a self-consistent variational calculation of all Feynmans' parameters we get quantum melting in a region in which  $\omega_{pol}$  do not actually soften. As a result the softening of internal polaronic frequency approaches quantum melting only asymptotically for very large  $\alpha$  (fig.2)..

Saturation occurs to value of  $r_c$  which seems to lie in the high density regime where our approach could be questionable. We must stress however that in the pure electron gas, the parameter  $r_s$  is a measure of *both* coupling and density. Indeed  $r_s$  can be obtained from the ratio of the Fermi energy to the mean Coulomb interaction, even if scaled with the band mass and the dielectric constant of the host medium, which are anyway fixed, i.e. no-density dependent. If we introduce another coupling

$\alpha$	$r_c$	$r_c^*$
1	510	99.8
3	334	99.3
5	168	99.5
7	46	99.8
9	20	197.5
11	15	452.2

TABLE I: The critical value at the melting of the density ( $r_c$ ) and coupling ( $r_c^*$ ) parameters as function of  $\alpha$  for high polarizability  $\eta = 0.16$ .

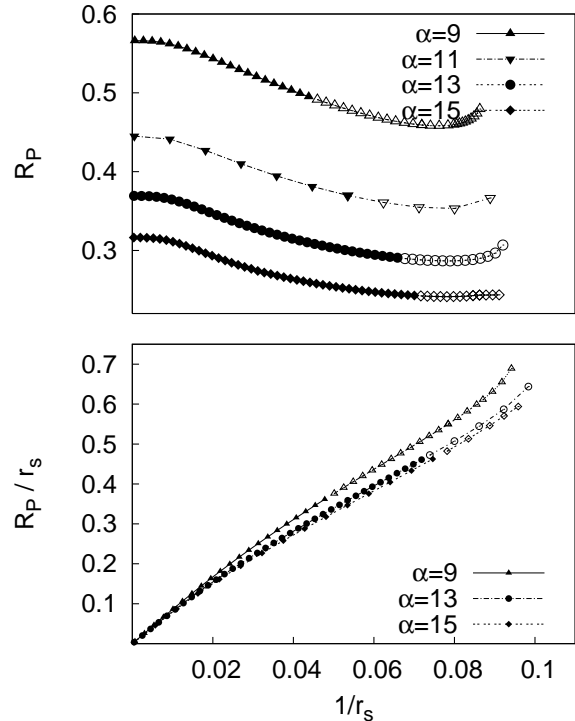


FIG. 4: Polaron radius in polaronic units (upper panel) and polaron radius scaled with  $r_s$  (lower panel) vs  $(1/r_s)$  (a.u.) for different  $\alpha$  and  $\eta = 0.17$  at low temperature ( $T = 5 \cdot 10^{-3}$  p.u.). Filled points refer to the solid phase.

in the system, as the e-ph interaction, the two concepts are distinct. Global interaction is not only a function of the density but it is also a function of the e-ph coupling  $\alpha$ . Now in the high polarizability case polarons are well defined as quasi-particles and we can use  $m_{pol}(\alpha)$  as effective mass while the repulsive interactions is screened by  $\epsilon_0$  in the low density regime. Only in this case we can introduce a measure of the *coupling* through the parameter  $r_s^* = (m_{pol}/\epsilon_0 m)r_s$ . For the low polarizability case the last assumption is not valid as explained onward. The values of  $r_s^*$  at the quantum melting ( $r_c^*$ ) are reported in tab.I. When the coupling  $\alpha < 7$  the quantum melting can be estimated thru eq.(43) which means  $r_c^* \simeq r_c(WC) = 100$  that is the *coupling* parameter  $r_c^*$  tends to the value of the Wigner crystal melting of a 3D electron-gas. On the contrary in the strong e-ph coupling the values of the effective coupling parameter  $r_c^*$  are much bigger than those of the density  $r_c$  due to the huge enhancement of the polaron mass.

Of course the exchange effects *at* the crystal melting are relevant and they can be taken into account only phenomenologically in our harmonic approximation (see footnote [42] and discussion in sec. II.C). However in the solid phase we must notice that these effects are ruled in

LPC by the parameter  $r_s^*$  rather than  $r_s$  making them much more negligible than those at the same density in the pure electron gas. To realize this fact we assume that the localized electronic wave function is a gaussian of variance  $\sigma$  then the overlap between two of these functions at distance  $r_s$  is proportional to  $\exp(-r_s^2/4\sigma^2)$ . Now  $\sigma$  in the harmonic approximation can be estimated as  $\sigma^2 = 1/2m_{pol}\omega_W$  where  $\omega_W^2 = \omega_{P,L}^2/3$  is the LPC Wigner frequency and  $\omega_{P,L}^2$  is given by eq. (2). Then is immediate to see that  $r_s^2/4\sigma^2 = \sqrt{r_s^*}/2$  a results that can be compared with the same for electron-gas [33] in which appears  $r_s$  and a different coefficient due to a more elaborate variational procedure. Taking into account data of table I we have that exchange effects are *a fortiori* negligible in a first approximation in the case of the strong e-ph coupling where the quantum melting occurs at huge coupling parameter  $r_c^*$ .

In fig. 4 we show the behavior of the polaron radius as a function of density. While in the solid phase it remains almost constant, when approaching the melting density it suddenly increases. This behavior can be understood by taking into account that the polaron radius is essentially determined by the diffusion in imaginary time of the electron path defined in eq.(92) of Appendix C (see also eqs.109,106 in Appendix E). Its maximum value occurs at  $\tau = \beta/2$  which diverges at the softening of the polaronic frequency ( $\omega_{pol} \sim 0$ ). Polaronic clouds tends to overlap (fig.4 lower panel). However, the polaronic nature of each particle of the LPC is preserved up to quantum melting.

#### d) Low polarizability: cross-over in solid phase

In this regime ( $\eta \sim 1$ ), the repulsive interactions among electrons overwhelm the attractive interactions due to the polarizability of the background, as can be seen by the relative weight of e-e and e-ph interaction coupling constant eqs.(11,12). However, self-trapping effects are still present at least at strong coupling and at low density, where electrons are localized.

Eq.(43) quantitatively describes quantum melting in the low polarizability case only at weak coupling ( $\alpha \leq 3$ ). When  $\alpha$  exceeds this value, a cross-over between a polaronic and a non polaronic phase is found inside the solid phase and the estimate of eq. (43) no longer describes quantum melting.

The low density regime, introduced in the previous subsection, is found only for the classical part of the crystal phase, where the polarization follows adiabatically the electron and the solid phase is a Wigner crystal made of polarons with an effective mass determined by the e-ph interaction, in the way discussed for high polarizability.

As far as the density increases (inside the solid phase), we observe that the two energy scale,  $\omega_{LO}$  of phonons and  $\omega_{P,L}$  and eq.(2) of the renormalized WC frequen-

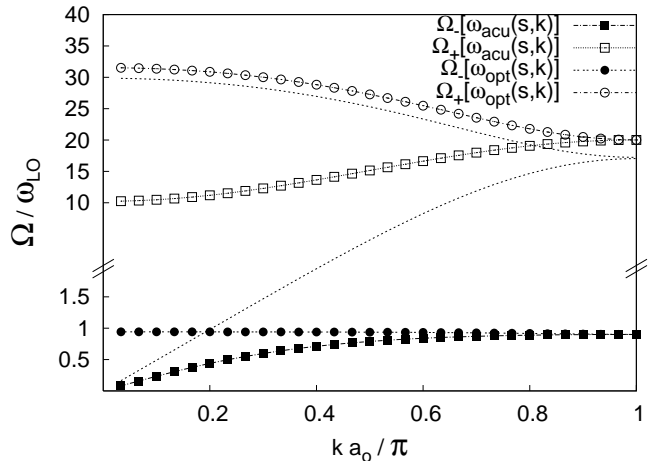


FIG. 5: Frequencies of the system in the simplified model as a function of  $\vec{k}$  along the direction (100), for  $\alpha = 5$  and  $\eta = 0.9$ , at  $1/r_s = 2.10^{-2}$  and at  $T = 1.8 \cdot 10^{-5}$  (a.u.). Density is close to the quantum melting. ( $\Omega_-[\omega_{acu}], \Omega_+[\omega_{acu}]$ ) result from the splitting of  $\omega_{acu}(s, k)$  the acoustical WC branch. ( $\Omega_-[\omega_{opt}], \Omega_+[\omega_{opt}]$ ) result from the splitting of the high frequency WC optical branch (eqs.(44,45)). For comparison are shown the pure WC frequencies (dotted lines).

cies, come close and we found a cross-over region *inside the solid phase*, where the electrons and the polarization modes are mixed as in the liquid phase CPPM (fig.1 of ref.[9] and fig.1 of ref.[10]). Example of the general situation is given in fig.5.

To estimate the density dependence of the LPC frequencies  $\Omega_{\pm}(\omega_{s,k})$ , let us substitute  $\omega_{s,\vec{k}}$  by the plasma frequency  $\omega_P$ . Results are reported in fig.6, which illustrates the density cross-over. In the low density limit ( $r_s \rightarrow \infty$ )  $\Omega_- = \omega_{P,L}$  eq.(2) while  $\Omega_+$  converges to  $\omega_{pol} \simeq v$ , the internal frequency for a single polaron. In this case, the electrons are far apart, and the “external” harmonic field generated by the surrounding electrons of the crystalline array is weak ( $K_e \sim e^2/r_s^3$ ). Therefore the frequency of electron oscillation ( $\omega_P^2 \sim K_e/m$ ) can be lower than that of the phonon ( $\omega_{LO}$ ), and the polarization follows the electron oscillation. The polaron vibrates as a whole with a lower frequency  $K_e/m_{pol} \sim \omega_P^2 (m/m_{pol}\epsilon_0)$ . The polarization charge distribution is undisturbed as a first approximation, so that the value of the internal polaronic frequency ( $\sim v$ ) of an electron inside its polarization well doesn’t change .

By increasing the density, we approach the opposite limit of strong external field. Now the frequency associated to this field is too large and the polarization cannot follow the electron oscillation, so that each electron becomes undressed from its polarization cloud. In this case  $\Omega_+$  approaches  $\omega_P/\sqrt{\epsilon_{\infty}}$ , the high density renormalized plasma frequency eq.(1), while  $\Omega_- \simeq \sqrt{\epsilon_{\infty}/\epsilon_0}\omega_{LO} =$

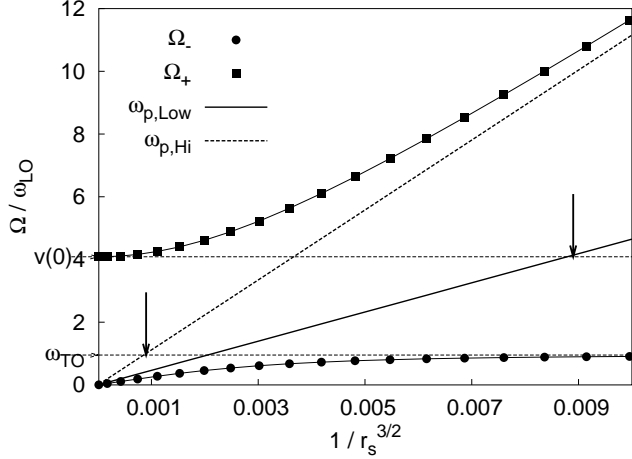


FIG. 6: Filled points are the typical frequencies of the simplified model obtained with  $\omega_{s,k} = \omega_P$  for  $\alpha = 5$  and  $\eta = 0.9$ . Solid line is the low density renormalized plasma frequency eq.(2). Dashed line the high density renormalized plasma frequency eq.(1). Arrows mark the crossover region (see text).

$\omega_{TO}$  is the characteristic renormalized frequency of the polarization. We notice that at low density  $\Omega_-$  gives a measure of the frequency of carrier density fluctuations, while in the opposite limit of high density, the same role is played by  $\Omega_+$ .

As we can see from fig.6, the cross-over amplitude is determined by the conditions  $\omega_{P,H} \simeq \omega_{TO}$  and  $\omega_{P,L} \simeq v$ . It is interesting to compare our fig.6 with the figure 1 of ref. [9]. We notice that the asymptotic boundary given there by the phonon frequency  $\omega_{LO}$  here it is played by the internal frequency.

The cross-over of the renormalization of the plasma frequency from low to high density regime doesn't imply the melting of the crystal. Indeed, it is observed within the boundary of the solid phase estimated by Lindemann criterion. This behavior is even more clear once we consider the fluctuations of the position of the electrons which enter in the Lindemann criterion.

The leading term for the Lindemann ratio at the classical melting is  $\delta_-^2 = \langle |u|^2 \rangle_- / d_{n.n.}^2$ , which is associated to the fluctuation of the center of mass eq.(37). Of course, in the classical region quantum fluctuations are ineffective, the electrons and its polarization cloud behave as a single classical particle with mass  $m_{pol}$ . The term  $\delta_+^2 = \langle |u|^2 \rangle_+ / d_{n.n.}^2$ , associated to the internal polaronic frequencies eq.(38) is indeed negligible.

To analyze the high density region where we meet eventually the Lindemann criterion for quantum melting, we notice that the condition  $\epsilon_{s,\vec{k}} \gg 1$ , where  $\epsilon_{s,\vec{k}}$  is defined in eq. (36), can be fulfilled by the majority of normal modes at high density. Of course, long wavelength acoustical

and even "optical" modes in 2D have vanishing energies, but their spectral weight is low enough to be neglected in the following considerations. Expanding  $\Omega_{\pm}(\omega_{s,k})$  in  $1/\epsilon_{s,\vec{k}}$  we get

$$\Omega_- \simeq \sqrt{\frac{\epsilon_{\infty}}{\epsilon_0}} \omega_{LO} \quad (44)$$

$$\Omega_+ \simeq \frac{\omega_{s,\vec{k}}}{\sqrt{\epsilon_{\infty}}} \quad (45)$$

In fig.5 the general solutions  $\Omega_{\pm}(\omega_{s,k})$  are shown for all the branches of the simplified model near the quantum melting.

The branches ( $\Omega_-[\omega_{opt}], \Omega_+[\omega_{opt}]$ ) which results as splitting of optical model of the Wigner crystal  $\omega_{opt}(s,k)$  are well described by approximation of eqs.(44,45).

The frequency dispersions ( $\Omega_-[\omega_{acu}], \Omega_+[\omega_{acu}]$ ) of the modes which originate from the splitting of acoustical branches of the Wigner crystal is also reported. While at short wavelength, the dispersion approaches the estimates given in eqs.(44,45) the long wavelength part of the spectrum is conversely described by the low density expansion  $\Omega_{\pm}$ .

Thus we have that at the quantum melting the low energy part of the spectrum still behaves as in the low density regime. The modes depicted in the lower part of fig.5 belongs to this part of the spectrum.

A measure of the wave-vector below which we have this behavior can be obtained by the condition  $\epsilon_{s,\vec{k}} = 1$ . The associated energy scale is given by  $\omega_c^2 = m\omega_{LO}^2 / (\epsilon_0 m_{pol})$ . Contrary to low density regime eqs.(37,38), it is not possible to associate to each term of the fluctuation eqs.(101,102) a definite degree of freedom. However, expanding the electron fluctuation with respect to the parameter  $\epsilon_{s,\vec{k}}$  for the frequencies  $\omega_{s,k} < \omega_c$  and with respect to the parameter  $1/\epsilon_{s,\vec{k}}$  for the frequencies  $\omega_{s,k} > \omega_c$  and using eq. (35) the electron position fluctuations can be approximated by:

$$\langle u^2 \rangle_- \simeq \int_0^{\omega_c} d\omega \rho(\omega) \frac{\hbar D \coth \left[ \hbar \left( \sqrt{\frac{m}{m_{pol}\epsilon_0}} \right) \omega / 2k_B T \right]}{2m_{pol} \left( \sqrt{\frac{m}{m_{pol}\epsilon_0}} \right) \omega} \quad (46)$$

$$\begin{aligned} \langle u^2 \rangle_+ &\simeq \left( \frac{M_T}{m + M_T} \right)^2 \frac{\hbar D}{2m\omega_{pol}} \coth \left( \frac{\hbar \omega_{pol}}{2k_B T} \right) \int_0^{\omega_c} d\omega \rho(\omega) \\ &+ \int_{\omega_c}^{\infty} d\omega \rho(\omega) \frac{\hbar D}{2m \frac{\omega}{\sqrt{\epsilon_{\infty}}}} \coth \left( \hbar \frac{\omega}{\sqrt{\epsilon_{\infty}}} / 2k_B T \right) \end{aligned} \quad (47)$$

Notice that the interpretation of the fluctuations associated to electronic motion in this case is different from that valid at low density. In particular the high energy contribution (the second term of eq. (47) represents a Wigner crystal-like fluctuation with a low energy cut-off. This is the largest contribution to the fluctuation at

quantum melting and does not depend on e-ph interaction.

Indeed the leading term of fluctuations at quantum melting is  $\langle u^2 \rangle_+$ . This is due to the vanishing of the spectral weight associated to the low frequencies  $\omega < \omega_c$  at high density (eq.(46)).

The saturation of the quantum melting point can be seen in the phase diagram of fig. 1 (lower panel). Two comments are needed. First, in the case of very low e-ph coupling, the density crossover does not occur inside the solid phase. Therefore, these arguments do not apply. The quantum melting point depends on the e-ph coupling as we have discussed in the previous section. However a saturation of the quantum melting density is observed clearly in fig.1 for intermediate and strong coupling. As a second point we have to emphasize that the quantum melting density *is not* that of a purely electronic Wigner crystal.

This fact can be explained by writing the total electron fluctuation as the sum of the two terms  $\langle u^2 \rangle_{Hi}$  and  $\langle u^2 \rangle_{Low}$  where  $\langle u^2 \rangle_{Hi}$  is the contribution to fluctuations of modes having energies higher (lower) than  $\omega_c$ . We notice from eq (47) that in both LPC and WC case  $\langle u^2 \rangle_{Hi}$  are the same. But while in the WC case the two terms are of the same order  $\langle u^2 \rangle_{Low} \simeq \langle u^2 \rangle_{Hi}$ , in the LPC case  $\langle u^2 \rangle_{Low} \ll \langle u^2 \rangle_{Hi}$  as far as the density increases. This is due to the renormalization of the low energy frequencies. Therefore, the electronic fluctuation in the LPC increases more slowly with density than those of the WC. At given density, the electronic fluctuation of the WC is greater than those of the LPC and this fact explains the shifting of the quantum melting toward higher densities.

The cross-over is also evident in the polaron radius. In the upper panel of fig. 7 we plot the polaron radius as defined by the eq.(34). We see that for any value of the e-ph coupling, the polaron radius tends to decrease as far as the density is increased. We recall that as far as the renormalized plasma frequency eq.(2) exceeds the phonon frequency, we enter in a region in which the polarization is adiabatically slow compared to the electronic motion. Therefore, the electronic charge appears as a static distribution whose radius decreases upon increasing the density and the polaron radius follows this trend. The crossover is evident by scaling the polaron radius with  $r_s$ , as reported in the lower panel of fig. 7 at intermediate and strong  $\alpha$ . Notice that as in the high polarizability case at the transition  $R_p/r_s \simeq 0.475$ .

It is possible to estimate the high density limit of the radial distribution of the induced charge. Using the condition  $\omega_o \ll \omega/\sqrt{\epsilon_\infty}$  we have the following expression valid at low temperature ( $k_B T \ll \hbar\omega_o$ ) (for details see

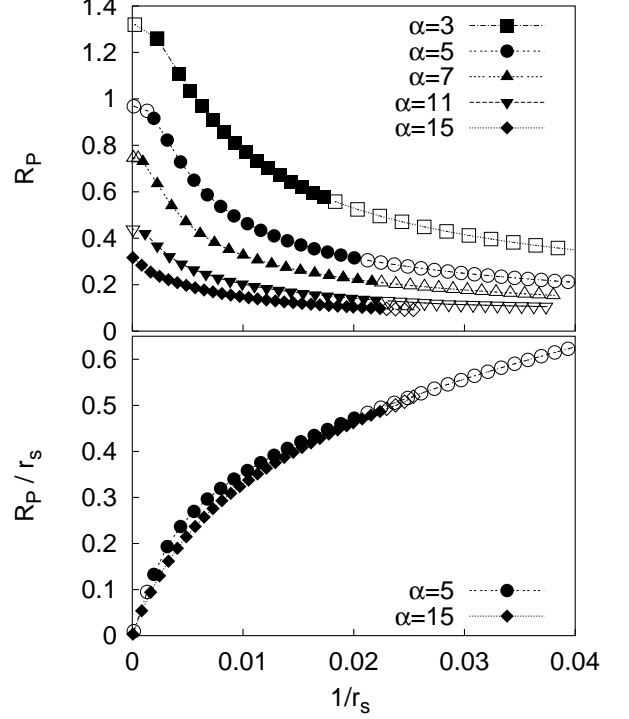


FIG. 7: Polaron radius in polaronic units (upper panel) and polaron radius scaled with  $r_s$  (lower panel) vs  $(1/r_s)$  (a.u.) for different  $\alpha$  in the case  $\eta = 0.9$  at low temperature ( $T = 5 \cdot 10^{-2}$  p.u.). Filled points refers to the solid phase.

Appendix E)

$$\tilde{g}(r) \simeq \frac{1}{\epsilon} \left[ \frac{r}{m\omega_{LO}} \left( 1 - \text{erf} \sqrt{\frac{r^2}{\langle u^2 \rangle}} \right) + \frac{2r^2}{\langle u^2 \rangle} \frac{e^{-\frac{r^2}{2\langle u^2 \rangle}}}{(2\pi \langle u^2 \rangle)^{3/2}} \right]. \quad (48)$$

The first term of eq. (48) takes into account quantum charge fluctuations which are relevant at small distances, while the remaining term is a classical contribution coming from the static charge distribution. Notice that only the first term depends on the e-ph interaction. Therefore, the polaron radius tends to the same high density asymptotic value for different values of the e-ph coupling  $\alpha$  (see upper panel of fig.7).

As a last point we notice that the cross-over condition, roughly estimated as  $\omega_P \sim \omega_{LO} \sim (1 - \eta)^2/\alpha^2 \sim 0.01/\alpha^2$ , shifts toward higher densities as the e-ph coupling constant  $\alpha$  is reduced. In the weak coupling regime it lies in the liquid phase where RPA approaches in both 3D refs.[22, 54] and in 2D case [55] can be applied. It is also worth to remark that for high polarizability and for all coupling the polaronic crossover is located in the liquid phase according to the highest value of  $\omega_{LO} \sim 0.7/\alpha^2$ .

### III - 2D CASE

The results obtained in the 2D case are qualitatively similar to the 3D case. Both the cross-over phenomenon in the low polarizability case and the softening of the polaronic frequency in the high polarizability case are observed. Results are reported in the zero temperature phase diagram of fig. 2. In this figure, we compare the phase diagrams in 2D and 3D by scaling appropriately the 2D e-ph coupling constant following the single polaron results of ref.[56]:  $\alpha_{3D} = (3\pi/4)\alpha_{2D}$ . 2D and 3D melting curves scale well according to the zero density scaling for all studied cases. A discrepancy is found in the the high polarizability strong e-ph coupling softening of  $\omega_{pol}$ . Let us first discuss the scaling at finite density.

In our variational scheme, the DOS of the WC is the peculiar difference between the 2D and 3D cases. To see this explicitly let us compare the e-ph interaction terms  $\mathcal{S}_{e-ph-e}^{self}$ . Assuming polaronic units we get:

$$\frac{1}{\beta} \frac{\langle \mathcal{S}_{e-ph-e}^{self} \rangle_{T,3D}}{3N} = -(\alpha) \frac{\sqrt{2}}{6} \int_0^{\frac{\beta}{2}} d\tau \frac{D_o(\tau)}{\sqrt{\frac{\pi}{2} d_{3D}(\tau)}} \quad (49)$$

$$\frac{1}{\beta} \frac{\langle \mathcal{S}_{e-ph-e}^{self} \rangle_{T,2D}}{2N} = -\left(\frac{3\pi}{4}\alpha\right) \frac{\sqrt{2}}{6} \int_0^{\frac{\beta}{2}} d\tau \frac{D_o(\tau)}{\sqrt{\frac{\pi}{2} d_{2D}(\tau)}} \quad (50)$$

where the imaginary-time diffusion  $d(\tau)$  eq.(92) is itself a functional of the DOS. We notice from eqs.(49,50) that the free energy functional scales explicitly as in the single polaron case [56] by scaling the coupling constant  $\alpha$ . Related to the different 2D and 3D DOS we remark the different behavior of the frequencies of the normal modes. Noticeably, the ‘‘optical’’ branches go to zero as  $\sim \sqrt{k}$  at long wavelengths [52]. As in the 3D case, the frequencies of the LPC are splitted in four branches (fig.8)  $\Omega_{\pm}[\omega_{acu}(s, \vec{k})]$  and  $\Omega_{\pm}[\omega_{opt}(s, \vec{k})]$  according to the same equation of 3D (see fig.8), where the 2D value for  $\omega_W$  is given in appendix B eq. (72).

Let us discuss the deviation from the the scaling at strong coupling, which we see from fig.2 in the density of the softening of the polaronic frequency  $\omega_{pol}$ . Actually we observe that a steep fall of the variational parameter  $v(r_s)$  occurs as density increases determining the softening of  $\omega_{pol}$ . Peculiar features of the DOS enters in the variational determination of  $v(r_s)$  as can be achieved by the following argument. First of all we assume that  $w$  is very close to the value  $\omega_{LO}$  at strong coupling. Then we notice that as in 3D high polarizability case the renormalized plasma frequency is much less than the phonon frequency and the discussion which follows eq. (36) holds for all densities lower than critical density of the softening. In this case the spectrum is composed by the low energy branches (renormalized WC) and the by polaronic branches weakly dispersed around  $v$  (see also fig.8). Us-

ing this results at low temperatures ( $\beta \rightarrow \infty$ ), the condition for the extrema of  $\mathcal{F}_V$  reads:

$$1 - \frac{1}{v^{3/2}} \sqrt{\frac{\omega_P^2}{w\varepsilon_o}} \mathcal{M}_2 + g(\alpha, \eta, r_s, v) = 0 \quad (51)$$

where the first and second terms are the derivative of  $\mathcal{F}_T$  eq.(89) and  $g$  is the derivative of eqs.(90,91,93) from Appendix C. As  $v(r_s) \rightarrow 0$  for  $r_s \simeq r_c$  the second term acquires importance and DOS enters in the second moment  $\mathcal{M}_2$ . However there are other terms which are divergent as  $v \rightarrow 0$  coming from the explicit form of the function  $g$ .

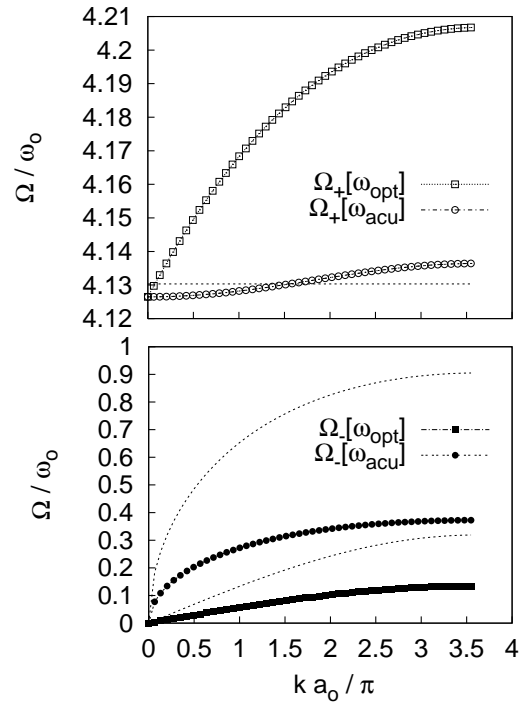


FIG. 8: 2D case. The eigenfrequencies of system along the direction (10) for  $\eta = 0.9$  and  $\alpha = 2.12$ .  $1/r_s = 8 \cdot 10^{-3}$  (a.u.),  $T = 2.5 \cdot 10^{-5}$  (a.u.). Density is close to the classical liquid-solid transition. Upper panel: The frequencies of polaronic branch weakly dispersed around the polaronic frequency  $\omega_{pol} \simeq v$  (dashed line). Lower panel: The renormalized Wigner crystal branches (points) and the pure WC branches (dashed lines).

### CONCLUSIONS

We have studied the behavior of a low density electron gas in the presence of a polarizable medium, where polaronic effects may play a relevant role. To determine

the transition line, we have used a generalized Lindemann criterion which reproduces correctly the pure electron gas quantum melting. Because the amplitude of quantum fluctuations depends on the e-ph renormalized plasma frequency, the Lindemann rule has been critically re-examined and adapted to the polaron crystal. This procedure allows to determine quantitatively the phase diagram of the model and to extend the study of the model to the low polarizability case, which was not studied before. We have also studied the 2D case, showing that the dimensional dependence is not crucial to determine the nature of the quantum melting within in our harmonic variational scheme. The scaling predicted for the e-ph coupling constant at zero density do apply as well at non zero density up to quantum melting. A noticeable difference instead is in the position of the density of the softening of the polaronic frequency which in 3D is much closer to the melting than in 2D case. This suggests that the hetero-interactions are less effective to destabilize the dipolar crystal in 2D. However other possible mechanism, (lattice-effects, structural disorder or impurities) can cooperate to the localization together with the interactions between the electrons and lead to the formation of a pinned Wigner Crystal. In this case the melting can not be predicted by the Lindemann rule but a similar dipolar instability due to the long-range interaction between the electrons can still drives the melting.

While the weak e-ph coupling regime is similar for both low and high polarization case, the strong coupling scenario is qualitatively different.

In the high polarizability regime, we have recovered the incipient instability which was found in previous studies near the solid phase [29, 30] and also in the liquid phase [31]. In comparison with previous work, we have found that this regime is restricted to very large values of the coupling  $\alpha > 10$  leaving an interesting intermediate region of coupling in which polarons may exist in the liquid phase. This region can in principle be explored with non perturbative numerical techniques as e.g. Path Integral Monte Carlo. Work along this direction is currently in progress.

In the low polarizability regime, a crossover occurs inside the solid phase when the renormalized plasma frequency approaches the phonon frequency. At low density, we still have a LPC, while at higher densities the electron-phonon interaction is weakened irrespective of the *bare* electron-phonon coupling. In this case, polaron clouds overlap as and the polaron feature of the crystal is lost. The crossover from polaronic ( $\omega_P < \omega_{LO}$ ) to non polaronic ( $\omega_P > \omega_{LO}$ ) character has been observed in weakly coupled systems such as GaAs in the liquid phase and analyzed in term RPA [22, 55]. In this system it occurs around  $r_s \sim 0.6 - 0.7$  while for ZnO  $\alpha$  is larger shifting the crossover to  $r_s \sim 7$ . Finding a system with low polarizability and larger e-ph coupling is difficult since it implies very low  $\omega_{LO}$ :  $\alpha \sim (1 - \eta)/\omega_{LO}$

from eq.(11). However in surfaces of InSb an  $\alpha = 4.5$  has been predicted together with  $\eta = 0.88$  [11] leading to the possible observation of the crossover inside the solid phase.

We notice also that our low polarizability scenario of density crossover inside the solid phase bear some resemblance to that found for ripplonic polaron systems [58]. Though the electron-ripplon interaction in these systems is different from the Fröhlich type, resonances in the absorption spectrum observed by Grimes and Adams [60], their explanation at low density [61] relies on the same qualitative arguments developed in the present work. Recent works on high density ripplonic polaron systems realized on a helium bubbles predicts also in this case a mixing between plasmon and polaron modes [62].

Finally we remark that we have obtained an appreciable stabilization of the crystal phase even for intermediate regime  $\alpha \sim 3 - 5$  in low polarizability cases. We conclude that the general result that e-ph interaction effects can stabilize the Wigner crystal phase could motivate experimental studies on two dimensional electronic devices involving polarizable media. To this aim a layered configuration is advised even with some warnings [63]. In 2D heterostructure the use of a perpendicular electric field [63] could not only increase the polaron effect but also tune it as it was shown in the case of charged helium surfaces [64].

## ACKNOWLEDGMENTS

Authors acknowledge S. Fratini and P. Quemerais for useful discussions and critical reading of the manuscript. We thanks also J. Lorenzana for useful suggestions. One of us (G.R.) thanks the also the kind hospitality of CNRS-LEPES Grenoble were a part of this work has been done.

This work was supported by MIUR-Cofin 2001 and MIUR-Cofin 2003 matching funds programs.

## APPENDIX A: THE LOW ENERGY CUT OFF IN 2D

The 2d DOS function can be defined as

$$\rho(\omega) = \sum_{s=1,2} \int_{V_B} d^2k \delta(\omega - \omega_{s,k}) \quad (52)$$

where  $V_B$  is the volume of the first Brillouin's zone (1BZ). Let us consider a small fraction  $\varepsilon$  of the plasma frequency  $\omega_P$ . At long wavelength ( $k = 0$ ), we have the 2D dispersion laws for the acoustical mode is  $\omega_1(k) \simeq c_1 k$  while the "optical"  $\omega_2(k) \simeq c_2 \sqrt{k}$  [46]. As a consequence the behavior of the DOS for  $\omega \simeq 0$  is

$$\int_0^{2\pi} d\theta \int_0^{k(\varepsilon)} dk k \delta(\omega - c_1 k) = \frac{2\pi}{c_1^2} \omega \quad (53)$$

$$\int_0^{2\pi} d\theta \int_0^{k(\varepsilon)} dk k \delta(\omega - c_2 \sqrt{k}) = \frac{4\pi}{c_2^4} \omega^3 \quad (54)$$

Introducing the scaled frequency  $x$  defined as  $\omega = \omega_P x$  and the quantum parameter  $\eta_q$  eq.(23), the thermal electronic fluctuation is expressed as an average on the DOS as

$$\langle u^2 \rangle = \frac{\hbar}{m} \left\langle \frac{\coth(\eta_q x)}{x} \right\rangle_{DOS} \quad (55)$$

$$= \frac{\hbar}{m} \int dx \rho(\omega_P x) \left[ \frac{1}{\eta_q x^2} + \eta_q (\alpha_0 + \alpha_2 (\eta_q x)^2 + \dots) \right] \quad (56)$$

Since  $\rho(\omega_P x) \sim x$  for  $x \rightarrow 0$ , the average in eqs. (55) converges for any of  $x^{2n}$  with  $n \geq 0$  in the the expansion eq.(56). In the  $n = -1$  term we consider infrared cut-off  $x_c$  giving

$$\begin{aligned} \left\langle \frac{1}{x^2} \right\rangle_{DOS} &\simeq \int_{x_c}^{\varepsilon} dx \frac{(2\pi/c_1^2)\omega_P}{x} + \int_{\varepsilon} dx \frac{\rho(\omega_P x)}{x^2} \\ &\simeq \frac{2\pi\omega_P}{c_1^2} \ln\left(\frac{\varepsilon}{x_c}\right) + \int_{\varepsilon} dx \frac{\rho(\omega_P x)}{x^2} \end{aligned} \quad (57)$$

This term diverges logarithmically as  $x_c \rightarrow 0$ . However  $\eta_q \rightarrow \infty$  as we approach the quantum region. The electronic fluctuation turns out to be cut-off independent if

$$\left\langle \frac{1}{x^2} \right\rangle \ll \eta_q^2 \left\langle \alpha_0 + \alpha_2 (\eta_q x)^2 + \dots \right\rangle. \quad (58)$$

We have chosen for the cut-off frequency  $x_c = \omega_{min}/\omega_P \simeq 5 \cdot 10^{-5}$  so that the condition eq.(58) is fulfilled around  $\eta_q(T, r_s) \geq 10$  which corresponds to a large region inside to the solid phase. By the relation for acoustical long wave excitation  $\omega_{min} = c_1 k_{min}$  and  $k_{min} = 2\pi/(r_s \sqrt{N})$ , the number of electrons is  $N = 5.24 \cdot 10^6$ . Our inverse second moment of DOS is  $\mathcal{M}_{-2} = 12.5$  (cfr ref. [53]  $\mathcal{M}_{-2} = 8.16$  for  $N = 1024$ ).

## APPENDIX B: THE HARMONIC VARIATIONAL APPROXIMATION

We expand in the harmonic approximation the terms  $\mathcal{S}_{e-e}, \mathcal{S}_{e-J}, \mathcal{S}_{e-ph-e}^{dist}$  (eqs.6,9,8). Let  $\vec{r}_i = \vec{R}_i + \vec{u}_i$ , where  $\vec{R}_i$  is the lattice point of the crystal and  $\vec{u}_i$  is the

electronic displacement from  $\vec{R}_i$ , and set  $\Delta \vec{u}_{i,j}(\tau, \sigma) = \vec{u}_j(\sigma) - \vec{u}_i(\tau)$  and  $\vec{R}_{j,i} = \vec{R}_j - \vec{R}_i$ . The static terms give

$$\mathcal{S}_{e-e}^o(\{\vec{R}_i\}) + \mathcal{S}_{e-J}^o(\{\vec{R}_i\}) + \mathcal{S}_{e-ph-e}^{o,dist}(\{\vec{R}_i\}) = \frac{\mathcal{S}_{WC}^o(\{\vec{R}_i\})}{\varepsilon_0} \quad (59)$$

the e-ph interaction does not change the equilibrium positions of the pure electronic crystal (WC) which corresponds to the minimum of the potential energy. The sum of the dynamical parts in the harmonic approximation gives

$$\begin{aligned} \mathcal{S}_{e-e}^H + \mathcal{S}_{e-J}^H + \mathcal{S}_{e-ph-e}^{H,dist} &= \\ = \int_0^\beta d\tau \sum_i [V_J(\vec{u}_i(\tau)) + V_{e-e}(\vec{u}_i(\tau))] &\quad (60) \end{aligned}$$

where

$$V_J(\vec{u}_i(\tau)) = -\frac{e^2 \rho_J}{\varepsilon_0} \int d^D r \left( \frac{1}{|\vec{u}_i(\tau) - \vec{r}|} - \frac{1}{r} \right) \quad (61)$$

$$V_{e-e}(\vec{u}_i(\tau)) = \frac{e^2}{2} \int_0^\beta d\sigma F(\tau - \sigma) \sum_{j \neq i} U_{j,i}(\tau, \sigma) \quad (62)$$

$$U_{j,i}(\tau, \sigma) = \frac{1}{2} \Delta \vec{u}_{i,j}(\tau, \sigma) \cdot \overline{\mathcal{I}}(\vec{R}_{j,i}) \Delta \vec{u}_{i,j}(\tau, \sigma) \quad (63)$$

$$F(\tau - \sigma) = \frac{\delta(\tau - \sigma)}{\varepsilon_\infty} - \frac{\omega_{LO}}{2\varepsilon} D_o(\tau - \sigma) \quad (64)$$

$$\left[ \overline{\mathcal{I}}_{ij} \right]_{\alpha\beta} = \frac{\delta_{\alpha\beta}}{|\vec{R}_{j,i}|^3} - 3 \frac{\left[ \vec{R}_{j,i} \right]_\alpha \left[ \vec{R}_{j,i} \right]_\beta}{|\vec{R}_{j,i}|^5} \quad (65)$$

From now we drop on the double  $\sigma, \tau$  indexes in  $\Delta \vec{u}_{i,j}$ . To evaluate the integral in eq.(61) and the sums on index  $j$  in eq.(62), we consider a sphere  $S_R$  of radius  $R_s$  (a disk in 2D) centered on site  $i$ . We first sum on index  $j$  and then we perform the limit  $R_s \rightarrow \infty$ . Finally we sum on index  $i$  in eq. (60).

### 3D case

By Gauss's law (with the condition  $V_J(0) = 0$ ), we have

$$V_J(\vec{u}_i(\tau)) = \frac{1}{2} m \frac{\omega_W^2}{\varepsilon_0} |\vec{u}_i(\tau)|^2 \quad (66)$$

where the Wigner frequency is  $\omega_W^2 = \omega_P^2/3$ . Because of  $V_J$  is independent of the size of  $S_R$ , eq.(66) does not change in the limit  $R_s \rightarrow \infty$ .

To evaluate the sum in eq.62 with the condition  $R_j < R_s$  we remind that we have two self terms ( $(i, i)$  and  $(j, j)$ ) and two distinct terms ( $(i, j)$  and  $(j, i)$ ) in eq. (63). The two self terms give the same contribution, as can be easily

check if we firstly we carry on the limit  $R_s \rightarrow \infty$  and then the sum on index  $j$  and  $i$ . They vanishes because of cubic symmetry of the lattice. When the two distinct terms  $((i, j)$  and  $(j, i))$  of eq. (63) are inserted in eq.(62) and the limit  $R_s \rightarrow \infty$  is taken, we obtain the term  $V_{e-e}(u_i)$  of eq.60

$$V_{e-e}(\vec{u}_i(\tau)) = \frac{e^2}{2} \sum_{j \neq i} \int_0^\beta d\sigma F(\tau - \sigma) \vec{u}_j(\sigma) \bar{\mathcal{I}}(\vec{R}_{j,i}) \vec{u}_i(\tau) \quad (67)$$

Summing on index  $i$  and integrating on variable  $\tau$  the eqs.(66,67), we obtain the terms  $\mathcal{S}_{e-J}^H, \mathcal{S}_{e-e}^H, \mathcal{S}_{e-ph-e}^{H,dist}$  eqs.(19,20).

### 2D case

In 2D the interaction potential  $V_J^R(u)$  of a uniform positive charged disk of radius  $R_s$  eq. (61) is

$$V_J^R(u) = -\frac{e^2 \rho_J}{\varepsilon_0} \int_0^{2\pi} d\theta F(\theta) \quad (68)$$

where

$$F(\theta) = \sqrt{R_s^2 + u^2 - 2R_s u \cos(\theta)} - u - R_s + u \cos(\theta) \ln \frac{R_s - u \cos(\theta) + \sqrt{R_s^2 + u^2 - 2R_s u \cos(\theta)}}{u(1 - \cos(\theta))}$$

In the limit  $R_s \rightarrow \infty$

$$\lim_{R \rightarrow \infty} V_J^R(\vec{u}_i) = \lim_{\frac{R}{u} \rightarrow 0} \frac{e^2}{\varepsilon_0} \rho_J \frac{\pi}{R_S} u_i^2 = 0 \quad (69)$$

since the total electric field of an infinite charged disk is perpendicular to the disk.

Then we have to evaluate the sums eq.(63). The two distinct terms  $((i, j)$  and  $(j, i))$  gives the identical result eq.67 of the 3D case while the self term  $(i, i)$  is written as

$$\frac{1}{2} \vec{u}_i \left( \sum_{\substack{\vec{R}_j < R \\ j \neq i}} \bar{\mathcal{I}}_{ij} \right) \vec{u}_i = \vec{u}_i \bar{\mathcal{D}} \vec{u}_i \quad (70)$$

the matrix  $\mathcal{D}$  in 2D is defined as sum of the matrices  $\bar{\mathcal{I}}(\vec{R}_j)$  eq.(65) on hexagonal lattice points  $\vec{R}_j$ . Contrary to the 3D case, the matrix  $\mathcal{D}$  is not zero in 2D case. By the lattice symmetry, the off-diagonal elements are zero while the diagonal terms are equal to the local potential which acts on each electrons

$$\frac{e^2}{2} \int_0^\beta d\sigma F(\tau - \sigma) \bar{\mathcal{D}}_{\alpha\alpha} |\vec{u}_i(\tau)|^2 = \frac{1}{2} m \frac{\omega_W^2}{\varepsilon_0} |\vec{u}_i(\tau)|^2 \quad (71)$$

where we use as definition 2D Wigner frequency

$$\omega_W^2 = \frac{e^2}{m} \lim_{R \rightarrow \infty} \sum_{\substack{j \neq i \\ R_{j,i} < R}} \frac{1}{2R_{j,i}^3} \quad (2D) \quad (72)$$

For an hexagonal lattice of nearest neighbor distance  $d_{n.n.}$ , we have  $\sum_{j \neq i} (1/2R_{j,i}^3) = 5.51709/d_{n.n.}^3$ . Summing on index  $i$  eqs.(67,71) we obtain the terms  $\mathcal{S}_{e-J}^H, \mathcal{S}_{e-e}^H, \mathcal{S}_{e-ph-e}^{H,dist}$  eqs.(19,20).

### Normal modes

The WC normal modes are defined as

$$\vec{u}_i = \frac{1}{\sqrt{N}} \sum_{\vec{k}, s} \hat{\varepsilon}_{\vec{k}, s} q_{\vec{k}, s} e^{i\vec{k} \cdot \vec{R}_i} \quad (73)$$

where the vectors  $\vec{k}$  belongs to the 1BZ of the reciprocal lattice,  $\hat{\varepsilon}_{\vec{k}, s}$  are eigenvector with eigenvalue  $\omega_{\vec{k}, s}^2$  of the dynamical matrix  $\bar{\mathcal{M}}$  which is defined as

$$\bar{\mathcal{M}}_{\alpha\beta} = \delta_{\alpha\beta} \omega_W^2 + \frac{e^2}{m} \sum_{\vec{R}_i \neq 0} \bar{\mathcal{I}}_{\alpha\beta}(\vec{R}_i) e^{i\vec{k} \cdot \vec{R}_i} \quad (74)$$

Inserting the WC normal modes eq.(73) in eqs.(16,18,19,20), we express the harmonic variational action  $\mathcal{S}_T$  as

$$\mathcal{S}_T(\{q_{s, \vec{k}}(\tau)\}) = \sum_{s, \vec{k}} \int_0^\beta d\tau L_{s, \vec{k}}(\tau) \quad (75)$$

where the Lagrangian is

$$L_{s, \vec{k}} = \frac{1}{2} m \left| \dot{q}_{\vec{k}, s}(\tau) \right|^2 + \frac{1}{2} m \frac{\omega_{\vec{k}, s}^2}{\varepsilon_0} \left| q_{\vec{k}, s}(\tau) \right|^2 + \frac{m w (v^2 - w^2)}{8} \int_0^\beta d\sigma D_V(\tau - \sigma) \left| q_{\vec{k}, s}(\tau) - q_{\vec{k}, s}(\sigma) \right|^2 + \frac{m \omega_{LO} (\omega_{\vec{k}, s}^2 - \omega_W^2)}{8\varepsilon} \int_0^\beta d\sigma D_o(\tau - \sigma) \left| q_{\vec{k}, s}(\tau) - q_{\vec{k}, s}(\sigma) \right|^2 \quad (76)$$

### APPENDIX C: THE VARIATIONAL FREE ENERGY $\mathcal{F}_V$

The first term of the variational free energy  $\mathcal{F}_V$  eq. (21) is the free energy  $\mathcal{F}_T$  associated to the partition function of the trial action  $\mathcal{Z}_T$ . This is calculated as the functional integral eq.(3) where  $\mathcal{S}_{eff}$  eq. (4) is replaced by  $\mathcal{S}_T$  eq. (17). The second term of  $\mathcal{F}_V$  is the mean value eq. (14) of the difference between  $\mathcal{S}_{e-ph-e}^{self}$  eq. (7) and  $\mathcal{S}_{Feyn}$  eq. (16).

We start by changing the dynamical variables of integration from  $\{\vec{u}_i(\tau)\}$  to  $\{q_{s, \vec{k}}(\tau)\}$ . By reality condition we



have  $q_{-\vec{k},s} = q_{\vec{k},s}^*$  and  $\hat{\varepsilon}_{-\vec{k},s} = -\hat{\varepsilon}_{\vec{k},s}$ , we must sum only  $\vec{k}$  vectors in the upper half space ( $k_z > 0$ ) of  $1BZ$

$$\vec{u}_i = \frac{1}{\sqrt{N}} \sum_{s,\vec{k},k_z>0} \hat{\varepsilon}_{\vec{k},s} \left[ q_{\vec{k},s} e^{i\vec{k}\vec{R}_i} - q_{\vec{k},s}^* e^{-i\vec{k}\vec{R}_i} \right] \quad (77)$$

Therefore the real and imaginary part of  $q_{s,\vec{k}}$  for all  $k$  with ( $k_z > 0$ ) of the  $1BZ$  are the actual independent variables and the Jacobian of canonical transformation is  $J = 2^{DN}$

$$\mathcal{Z}_T = \int J \prod_{s,\vec{k},k_z>0} \mathcal{D}[q_{s,\vec{k}}^{Re}(\tau)] \mathcal{D}[q_{s,\vec{k}}^{Im}(\tau)] e^{-\mathcal{S}_T\{q_{s,\vec{k}}(\tau)\}} \quad (78)$$

Using the periodicity condition ( $q_{s,\vec{k}}(0) = q_{s,\vec{k}}(\beta)$ ), we have the following Fourier expansion ( $\omega_n = (2\pi/\beta)n$ )

$$q_{s,\vec{k},n} = \frac{1}{\beta} \int_0^\beta d\tau q_{s,\vec{k}}(\tau) e^{-i\omega_n \tau} \quad (79)$$

$$q_{s,\vec{k}}(\tau) = q_{s,\vec{k},c} + \delta q_{s,\vec{k}}(\tau) \quad (79)$$

$$q_{s,\vec{k},c} = \frac{1}{\beta} \int_0^\beta d\tau q_{s,\vec{k}}(\tau) \quad (80)$$

$$\delta q_{s,\vec{k}}(\tau) = \sum_{\substack{n=-\infty \\ n \neq 0}}^{\infty} q_{s,\vec{k},n} e^{i\omega_n \tau} \quad (81)$$

where we have separated the mean value of path on the imaginary time eq.(80) (centroid) from the fluctuation around it eq.(81). The action  $\mathcal{S}_T(\{q_{s,\vec{k}}(\tau)\})$  is quadratic in  $\{q_{s,\vec{k},n}\}$  therefore we can separate eq.(78) in two gaussian integrals

$$\mathcal{Z}_T = \mathcal{Z}_{T,c} \mathcal{Z}_{T,\delta q} \quad (82)$$

$$\begin{aligned} \mathcal{Z}_{T,c} &= \int \prod_{s,\vec{k},k_z>0} \frac{dq_{\vec{k},s,c}^{Re} dq_{\vec{k},s,c}^{Im}}{\pi \hbar^2 / mk_B T} e^{-\mathcal{S}_T\{q_{s,\vec{k},c}\}} \\ &= \int \prod_{s,\vec{k},k_z>0} \frac{dq_{\vec{k},s,c}^{Re} dq_{\vec{k},s,c}^{Im}}{\pi \hbar^2 / mk_B T} e^{-\frac{m}{k_B T} \frac{|q_{\vec{k},s,c}|^2}{s,\vec{k}'/\varepsilon_0}} \\ &= \prod_{s,\vec{k}} \frac{k_B T}{\hbar \omega_{s,\vec{k}} / \sqrt{\varepsilon_0}} \end{aligned} \quad (83)$$

hence after we omit the classic term  $\mathcal{Z}_{T,c}$  eq.(83).

$$\begin{aligned} \mathcal{Z}_{T,\delta q} &= \int \prod_{\substack{n \neq 0 \\ s,\vec{k},k_z>0}} \frac{dq_{\vec{k},s,n}^{Re} dq_{\vec{k},s,n}^{Im}}{\pi k_B T / m \omega_n^2} e^{-\delta \mathcal{S}_T\{\delta q_{s,\vec{k}}(\tau)\}} \\ &= \int \prod_{\substack{n \neq 0 \\ s,\vec{k},k_z>0}} \frac{dq_{\vec{k},s,n}^{Re} dq_{\vec{k},s,n}^{Im}}{\pi k_B T / m \omega_n^2} e^{-\frac{m}{k_B T} \frac{|q_{\vec{k},s,n}|^2}{\lambda_{s,\vec{k},n}}} \\ &= \prod_{\substack{n \neq 0 \\ s,\vec{k},k_z>0}} \omega_n^2 \lambda_{s,\vec{k},n} \end{aligned} \quad (84)$$

where

$$\lambda_{s,\vec{k},0} = \frac{1}{\omega_{\vec{k},s}^2 / \varepsilon_0} \quad (85)$$

$$\lambda_{s,\vec{k},n} = \sum_{\gamma=1}^3 \frac{A_\gamma}{\omega_n^2 + \Omega_\gamma^2} \quad (86)$$

$$A_1 = \frac{(\Omega_1^2 - \omega_{LO}^2)(\Omega_1^2 - w_T^2)}{(\Omega_1^2 - \Omega_2^2)(\Omega_1^2 - \Omega_3^2)} \quad (\text{cyclic perm. } \gamma = 1, 2, 3) \quad (87)$$

the frequencies  $\Omega_\gamma^2$  ( $\gamma = 1, 2, 3$ ) are the opposite of the roots of cubic

$$\mathcal{P}_3(z) = z^3 + a_2 z^2 + a_1 z + a_0 \quad (88)$$

$$a_2 = v^2 + \omega_{LO}^2 + \frac{\omega_{\vec{k},s}^2}{\varepsilon_0} + \frac{\omega_{\vec{k},s}^2 - \omega_W^2}{\bar{\varepsilon}}$$

$$a_1 = \omega_{LO}^2 v^2 + \frac{\omega_{\vec{k},s}^2}{\varepsilon_0} (\omega_{LO}^2 + w^2) + w^2 \frac{\omega_{\vec{k},s}^2 - \omega_W^2}{\bar{\varepsilon}}$$

$$a_0 = \frac{\omega_{LO}^2 w^2 \omega_{\vec{k},s}^2}{\varepsilon_0}$$

The gaussian integrals eq.(84) are convergent if  $\lambda_{s,\vec{k},n}$  are positive numbers  $\forall (s, \vec{k}, n)$ . This condition is fulfilled if  $\Omega_\gamma^2$  are all positive. The numerical minimization of the variational free energy has been made enforcing this constraint. Performing the infinite product in eq.(84) we have

$$\begin{aligned} \mathcal{Z}_{T,\delta q} &= \left( \frac{\sinh(\hbar \omega_{LO} / 2k_B T)}{\hbar \omega_{LO} / 2k_B T} \right)^{DN} \left( \frac{\sinh(\hbar w / 2k_B T)}{\hbar w / 2k_B T} \right)^{DN} \\ &\cdot \prod_{s,\vec{k},\gamma} \frac{\hbar \Omega_{\gamma,s,\vec{k}} / 2k_B T}{\sinh(\hbar \Omega_{\gamma,s,\vec{k}} / 2k_B T)} \end{aligned}$$

and finally we substitute the sum on  $(\vec{k}_i, s)$  with the integral on the WC DOS  $\rho(\omega)$  in the free energy  $\mathcal{F}_T$

$$\begin{aligned} \frac{\mathcal{F}_T}{DN} &= -k_B T \ln \left[ \sinh \left( \frac{\hbar \omega_{LO}}{2k_B T} \right) \sinh \left( \frac{\hbar w}{2k_B T} \right) \right] \\ &+ k_B T \int d\omega \rho(\omega) \sum_{\gamma=1}^3 \ln \left[ \sinh \left( \frac{\hbar \Omega_\gamma(\omega)}{2k_B T} \right) \right] \end{aligned} \quad (89)$$

To calculate the mean value of  $\mathcal{S}_{e-ph-e}^{self}$  eq. (7) in  $3D$  we use the following identity [57]

$$\begin{aligned} \iint_0^\beta d\tau d\sigma D_o(\tau - \sigma) \int \frac{d^3 q}{(2\pi)^3} \frac{4\pi}{q^2} \left\langle e^{i\vec{q} \cdot [\vec{u}_i(\tau) - \vec{u}_i(\sigma)]} \right\rangle_T &= \\ &= -2\beta \int_0^{\frac{\beta}{2}} d\tau \frac{D_o(\tau)}{\sqrt{\frac{\pi}{2}} d_{3D}(\tau)} \end{aligned} \quad (90)$$

while in  $2D$  ( $q^2 = q_{\perp}^2 + q_z^2$ )

$$\begin{aligned} \iint_0^{\beta} d\tau d\sigma D_o(\tau - \sigma) \int \frac{d^2 q_{\perp}}{(2\pi)^2} \frac{2\pi}{q_{\perp}} e^{-\frac{1}{2}d_{2D}(\tau - \sigma)q_{\perp}^2} &= \\ &= -2\beta \left(\frac{\pi}{2}\right) \int_0^{\frac{\beta}{2}} d\tau \frac{D_o(\tau)}{\sqrt{\frac{\pi}{2}d_{2D}(\tau)}} \end{aligned} \quad (91)$$

where  $d_D(\tau)$  is the imaginary time diffusion in the LPC defined as (3D or 2D)

$$d_D(\tau) = \frac{\langle |\vec{u}(\tau) - \vec{u}(0)|^2 \rangle_T}{D} \quad (92)$$

The mean value of  $\mathcal{S}_{Feyn}$  eq. (16) is

$$\begin{aligned} \langle \mathcal{S}_{Feyn} \rangle_T / N &= \\ &= -D \frac{mw(v^2 - w^2)}{8} \iint_0^{\beta} d\tau d\sigma D_T(\tau - \sigma) d_D(\tau - \sigma) \end{aligned} \quad (93)$$

To obtain eqs.(90,91,93) we have used

$$\left\langle e^{i\vec{q} \cdot [\vec{u}_i(\tau) - \vec{u}_i(\sigma)]} \right\rangle_T = e^{-\frac{1}{2}d_D(\tau - \sigma)q^2} \quad (94)$$

We will demonstrate eq.(94) in the next subsection.

#### Calculation of $\langle \exp(i\vec{q} \cdot [\vec{u}_i(\tau) - \vec{u}_i(\sigma)]) \rangle_T$

From eqs.(73,81) we have

$$i\vec{q} \cdot [\vec{u}_i(\tau) - \vec{u}_i(\sigma)] = \sum_{\substack{s, k_z > 0 \\ n \neq 0}} \left[ q_{\vec{k}, s, n} J_{s, k, n}^*(\tau - \sigma, \vec{q}) + c.c. \right] \quad (95)$$

$$J_{s, k, n}^*(\tau - \sigma, \vec{q}) = \frac{i}{\sqrt{N}} \vec{q} \cdot \hat{\varepsilon}_{\vec{k}, s} (e^{i\omega_n \tau} - e^{i\omega_n \sigma}) e^{i\vec{k} \cdot \vec{R}_i} \quad (96)$$

then we have

$$\begin{aligned} \langle \exp(i\vec{q} \cdot [\vec{u}_i(\tau) - \vec{u}_i(\sigma)]) \rangle_T &= \\ &= \frac{1}{Z_{T, \delta q}} \prod_{\substack{n \neq 0 \\ s, \vec{k}, k_z > 0}} \frac{dq_{\vec{k}, s, n}^{Re} dq_{\vec{k}, s, n}^{Im}}{\pi k_B T / m \omega_n^2} e^{-\frac{m}{k_B T} \frac{|q_{\vec{k}, s, n}|^2}{\lambda_{s, \vec{k}, n}} + q_{\vec{k}, s, n} J_{\vec{k}, s, n}^* + c.c.} \\ &= \prod_{\substack{s, k_z > 0 \\ n \neq 0}} e^{-\frac{k_B T}{m} \lambda_{s, \vec{k}, n} |J_{\vec{k}, s, n}|^2} = e^{-\frac{1}{2} \frac{1}{N} \sum_{s, k} |\hat{q} \cdot \hat{\varepsilon}_{\vec{k}, s}|^2 d_{\omega_{s, k}}(\tau - \sigma) q^2} \\ &= e^{-\frac{1}{2} \frac{1}{ND} \sum_{s, k} d_{\omega_{s, k}}(\tau - \sigma) q^2} = e^{-\frac{1}{2} d_D(\tau - \sigma) q^2} \end{aligned}$$

where the component of frequency  $\omega_{s, k}$  of the imaginary time diffusion  $d_D(\tau)$  is ( $A_{\gamma} = A_{\gamma}(\omega_{s, k})$ ,  $\Omega_{\gamma} = \Omega_{\gamma}(\omega_{s, k})$ )

$$\begin{aligned} d_D(\tau) &= \frac{1}{ND} \sum_{s, k} d_{\omega_{s, k}}(\tau) \\ &= \frac{1}{ND} \sum_{s, k} \frac{\hbar}{m} \sum_{\gamma} \frac{A_{\gamma} \cosh(\beta \Omega_{\gamma} / 2) - \cosh(\Omega_{\gamma} [\beta / 2 - \tau])}{\sinh(\beta \Omega_{\gamma})} \end{aligned} \quad (98)$$

## APPENDIX D: MEAN ELECTRONIC FLUCTUATION

The relation between the mean electronic fluctuation and the imaginary time diffusion  $d_D(\tau)$  eq.(92) is

$$d_D(\tau) = \frac{2}{D} \left[ \langle |\vec{u}(0)|^2 \rangle - \langle \vec{u}(\tau) \cdot \vec{u}(0) \rangle \right] \quad (99)$$

comparing eq.(99) and eq.(98) for  $d_D(\tau)$  and inserting the DOS function, we have

$$\sigma_T^2 = \frac{\langle |\vec{u}|^2 \rangle}{D} = \int d\omega \rho(\omega) \sum_{\gamma=1}^3 \frac{\hbar A_{\gamma}(\omega)}{2m\Omega_{\gamma}^2(\omega)} \coth\left(\frac{\beta \Omega_{\gamma}(\omega)}{2}\right) \quad (100)$$

If we fix  $w = \omega_o$ , we have  $\Omega_3 = \omega_o$  for one solution of the cubic polynomial eq.(88) and by eq.(87) we have also  $A_3 = 0$ . The other two terms give

$$\langle u^2 \rangle_+ = \int d\omega \rho(\omega) \frac{\Omega_1^2 - \omega_{LO}^2}{\Omega_1^2 - \Omega_2^2} \frac{\hbar D}{2m\Omega_1} \coth\left(\frac{\hbar \Omega_1}{2k_B T}\right) \quad (101)$$

$$\langle u^2 \rangle_- = \int d\omega \rho(\omega) \frac{\Omega_2^2 - \omega_{LO}^2}{\Omega_2^2 - \Omega_1^2} \frac{\hbar D}{2m\Omega_2} \coth\left(\frac{\hbar \Omega_2}{2k_B T}\right) \quad (102)$$

Notice that if we take a single Wigner frequency being representative of the electronic spectrum ( $\rho(\omega) = \delta(\omega - \omega_W)$ ) we recover the results of ref. [29].

## APPENDIX E: POLARON RADIUS

We now calculate the density-density correlation function of the eq.(32) for the variational harmonic action  $\mathcal{S}_T$ . We assume that the equilibrium position of the reference electron  $i = 1$  is the origin. With the same method to obtain eqs.(97), we performed the following Gaussian integrals for the density distribution  $\rho_1(\vec{r})$

$$\langle \hat{\rho}_1(\vec{r}) \rangle_T = \int \frac{d^D q}{(2\pi)^D} e^{i\vec{q} \cdot \vec{r}} \langle e^{i\vec{u}_1 \cdot \vec{q}} \rangle_T = \frac{e^{-r^2/2\sigma_T^2}}{[2\pi\sigma_T^2]^{D/2}} \quad (103)$$

and

$$\left\langle e^{-i\vec{q} \cdot \vec{u}_1} e^{i\vec{q} \cdot (\vec{u}_1(\tau) - \vec{u}_1)} \right\rangle_T = e^{-\frac{\sigma_T^2}{2} q^2} e^{-\frac{d(\tau)}{2} \vec{q} \cdot [\vec{q} + \vec{q}]} \quad (104)$$

(97) Inserting eq.(104) in eq.(32), we have the density-density correlation function in the imaginary-time for the  $i = 1$  electron

$$\left\langle \rho_1(\vec{r}) \rho_1(\vec{r}', \tau) \right\rangle_T = \langle \hat{\rho}_1(\vec{r}) \rangle_T \frac{e^{-\frac{|\vec{r} - \vec{r}' + \frac{d(\tau)}{2\sigma_T^2} \vec{r}'|^2}}{2\ell^2(\tau)}}{(2\pi\ell^2(\tau))^{D/2}} \quad (105)$$

where

$$\ell^2(\tau) = d_D(\tau) \left[ 1 - \frac{d_D(\tau)}{4\sigma_T^2} \right] \quad (106)$$

We notice that the function of eq.(105) does not depend only on the relative distance  $\vec{r}^j - \vec{r}$  but also from the distance of electron from its localization position in the crystal. Then the eq.(32) becomes

$$C_{1,T}^{self} = \frac{1}{\bar{\epsilon}} \int_0^\beta d\tau \frac{\omega_{LO}}{2} D_o(\tau) \frac{\langle \rho_1(\vec{r}) \rho_1(\vec{r}^j, \tau) \rangle_T}{\langle \rho_1(\vec{r}) \rangle_T} \quad (107)$$

We assume  $\vec{r} = 0$  (electron in its lattice point) and then we obtain the variational radial induced charge density

$$g_T(r) = \frac{\pi\omega_{LO}}{2\bar{\epsilon}} (2r)^{D-1} \int_0^\beta d\tau D_o(\tau) \frac{e^{-r^2/2\ell^2(\tau)}}{(2\pi\ell^2(\tau))^{3/2}} \quad (108)$$

by eq.(34) we obtain the variational polaron radius

$$R_{p,T} = \left( D \frac{\omega_{LO}}{2} \int_0^\beta d\tau D_o(\tau) \ell^2(\tau) \right)^{1/2} \quad (109)$$

### High density limit

The characteristic length  $\ell^2(\tau)$  defined in eq.(106) is expressed in term of  $\tau$ -dependent positional fluctuations  $d_D(\tau)$ , eq.(92), which is an integral of a function  $d_{\omega_s,k}(\tau)$  weighted by the DOS  $\rho(\omega)$  of the Wigner lattice, eq.(98). To have an estimate of this integral we replace the integration by inserting an average frequency in the function  $d_{\omega_s,k}$ . We choose  $\omega_P/\sqrt{\epsilon_\infty}$  because it is the typical frequency of the electronic fluctuation in the crystal for the high density regime eq. (47). Moreover we consider the low temperature limit ( $k_B T \ll \hbar\omega_P/\sqrt{\epsilon_\infty}$ ). Then from eq.(106) we get the following estimate for  $\ell^2(\tau)$

$$\ell^2(\tau) \simeq \frac{\hbar}{m\omega_P/\sqrt{\epsilon_\infty}} \left( 1 - e^{-2\frac{\omega_P}{\sqrt{\epsilon_\infty}}\tau} \right) \quad (110)$$

The characteristic time scale of electronic diffusion in imaginary time is  $\tau_{el} = (\omega_P/\sqrt{\epsilon_\infty})^{-1}$ . The rising-time is  $\tau_{el} = 1/(2\omega_P/\sqrt{\epsilon_\infty})$ . Therefore we have approximately

$$\begin{aligned} \ell^2(\tau) &\simeq \frac{\hbar}{m}\tau \quad (\tau \ll \tau_{el}) \\ \ell^2(\tau) &\simeq \frac{\hbar}{2m\frac{\omega_P}{\sqrt{\epsilon_\infty}}} \quad (\tau \gg \tau_{el}) \end{aligned}$$

Now in the variational polaron radius  $R_{p,T}$  of eq.(109) another time scale appears  $\tau_{ph} = \omega_{LO}^{-1}$  but at high density  $\tau_{ph} \gg \tau_{el}$ . Now we can separate the lowest time scale  $\tau_{el}$  contribution in the imaginary time integral so that we

can approximate the integral in eq.(109) as

$$\begin{aligned} \int_0^{\tau_{el}} d\tau D_o(\tau) \frac{e^{-\frac{r^2}{2\ell^2(\tau)}}}{(2\pi\ell^2(\tau))^{3/2}} &\simeq D_o(0) \int_0^{\tau_{el}} d\tau \frac{e^{-\frac{r^2}{2\frac{\hbar}{m}\tau}}}{(2\pi\ell^2(\tau))^{3/2}} \\ &= \frac{m}{2\pi\hbar} \frac{1}{r} \left( 1 - \text{erf} \sqrt{\frac{r^2}{\langle u^2 \rangle}} \right) \\ \int_{\tau_{el}}^\beta d\tau D_o(\tau) \frac{e^{-\frac{r^2}{2\ell^2(\tau)}}}{(2\pi\ell^2(\tau))^{3/2}} &\simeq \frac{e^{-\frac{r^2}{m\omega_P/\sqrt{\epsilon_\infty}}}}{(2\pi\langle u^2 \rangle)^{3/2}} \int_{\tau_{el}}^\beta d\tau D_o(\tau) \\ &\simeq \frac{e^{-r^2/2\langle u^2 \rangle}}{(2\pi\langle u^2 \rangle)^{3/2}}. \end{aligned}$$

Collecting these results we get eq. (48).

- 
- [1] E. Wigner, Phys. Rev. **46**, 1002 (1934).
  - [2] Jongsoo Yoon, C. C. Li, D. Shahar, D. C. Tsui and M. Shayegan Phys. Rev. Lett. **82**, 1744 (1998).
  - [3] M. D. Jones, D. M. Ceperley, Phys. Rev. Lett. **76** 4572 (1996).
  - [4] Bernu B., Cândido L., Ceperley D. M. Phys. Rev. Lett. **86**, 870 (2001).
  - [5] S. T. Chui, B. Tanatar, Phys. Rev. Lett. **74**, 458 (1995).
  - [6] *Polarons and Excitons*, C. G. Kuper and G. D. Whitfield edits. (Oliver and Boyd, Edinburgh, 1962).
  - [7] *Polarons in Ionic Crystals and Polar semiconductor* (edition par. J. Devreese, Amsterdam, North Holland, 1972).
  - [8] A. Mooradian, G. B. Wright Phys. Rev. Lett. **16**, 999 (1966).
  - [9] B. B. Varga Phys. Rev. A **137**, 1896 (1965).
  - [10] G. Irmer, M. Wenzel, J. Monecke Phys. Rev. B **56**, 9524 (1997) and refs. therein.
  - [11] Hong Sun, Shi-Wei Gu, Phys. Rev. B **44** 1163 (1991).
  - [12] Peng Zhang, Wei Xiao, Jing-Lin Xiao, Physica B **245**, 354 (1998).
  - [13] N. Kirova, M. N. Bussac, Phys. Rev. B **68** 235312 (2003), N. Kirova, M. N. Bussac, J. Phys. IV France **12** 99 (2002).
  - [14] Y. H. Kim, C. M. Foster, A. J. Heeger, S. Cox and G. Stucky, Phys. Rev. B **38**, 6478 (1988).
  - [15] C. Taliani, R. Zambone, G. Raum, F. C. Matocotta and K. I. Pokhadnya, Solid State Commun. **66**, 487 (1988).
  - [16] S. Lupi, P. Calvani, M. Capizzi, P. Maselli, W. Sadowski and E. Walker, Phys. Rev. B **45**, 12470 (1992); P. Calvani, M. Capizzi, S. Lupi, P. Maselli, A. Paolone and P. Roy, Phys. Rev. B **53**, 2756 (1996).
  - [17] A. Lanzara, P. V. Bogdanov, X. J. Zhou, S. A. Kellar, D. L. Feng, E. D. Lu, T. Yoshida, H. Eisaki, A. Fujimori, K. Kishio, J. -I. Shimoyama, T. Noda, S. Uchida, Z. Hussain and Z. X. Shen, Nature **412**, 510-514 (2001).
  - [18] S. Fratini, P. Quémerais, Mod. Phys. Lett. B **12** 1003 (1998).
  - [19] M. A. Kastner, R. J. Birgeneau, G. Shirane, Y. Endoh, Rev. Mod. Phys. **70** p.897 (1998).
  - [20] Lucarelli, A. Lupi, S. Ortolani, M. Calvani, P. Maselli, P. Capizzi, M. Giura, P. Eisaki, H. Kikugawa, N. Fujita, T. Fujita, M. Yamada, K. Phys. Rev. Lett. **90**, 037002 (2003).
  - [21] A. V. Puchkov, T. Timusk, M. A. Karlow, S. L. Cooper, P. D. Han, D. A. Payne Phys. Rev. B **54** 6686 (1996).

- [22] G. D. Mahan, *Many-Particle physics*, (Plenum, New York 1981) chap. 6; G. D. Mahan, in ref. [7] p.553.
- [23] L. F. Lemmens, J. T. Devreese, F. Brosens Phys. stat. sol. (b) **82**, 439 (1977).
- [24] G. Iadonisi, G. Capone, V. Cataudella, G. De Filippis Phys. Rev. B **53** 13497 (1996).
- [25] I. Bozovic Phys. Rev. B **48**, 876 (1993).
- [26] G. De Filippis, V. Cataudella, G. Iadonisi Eur. Phys. J. **8** 339 (1999).
- [27] T. D. Lee, F. Low, D. Pines, Phys. Rev. **90**, 297 (1953).
- [28] P. Quémerais Mod. Phys. Lett. B **9**, 1665 (1995).
- [29] S. Fratini, P. Quémerais, Eur. Phys. J. B **14**, 99 (2000).
- [30] S. Fratini, P. Quémerais, Eur. Phys. J. B **29**, 41 (2002).
- [31] J. Lorenzana, Europhys. Lett. **53**, 532 (2001).
- [32] p.29-80 of ref. [6]
- [33] W. J. Carr Phys. Rev. **122** 1437 (1961).  
See also sect. II.
- [34] R. P. Feynman, A. R. Hibbs *Quantum Mechanics and Path Integrals* (McGraw-Hill, 1965).
- [35] G. Verbist, M. A. Smondyrev, F. M. Peeters, J. T. Devreese, Phys. Rev. B **45**, 5262 (1992),
- [36] The pure electron gas limit of action eq.(4) can be reached when  $\alpha = 0$  and  $\alpha_e$  is finite, which implies  $\eta = 1$ . On the other hand, for a given  $\eta$ ,  $\alpha_e \rightarrow 0$  as  $\alpha \rightarrow 0$ . It should be noted, however, that the limit of zero e-ph interaction is somehow unphysical in the presence of a given inverse polarizability parameter of the system: as can be seen by the calculation of appendix B, when  $\varepsilon_0 \neq \varepsilon_\infty$ , the interaction with the polarizable medium is necessary to stabilize the crystal phase (static term).
- [37] R. P. Feynman, Phys. Rev. **97**, 660 (1955).
- [38] T. D. Schultz, Phys. Rev. **116**, 526 (1969).
- [39] R. Mochkovitch, J. P. Hansen Phys. Lett. **73 A** n.1, p.35 (1979).
- [40] Hitose Nagara, Yoichi Nagata and Tuto Nakamura, Phys. Rev. A **36**, 1859 (1987). (See also footnote [31]).
- [41] D. Ceperley private communication, see also ref. [4].
- [42] In this sense the stabilization of the solid phase due to Fermi statistics is here considered not explicitly, since we consider distinguishable particles, but phenomenologically via the fitted parameter  $\gamma(\eta_q)$ .
- [43] Notice however that this discussion does not involve the l.h.s. of eq.(22) in which  $\omega_P$  appears as a result of harmonic approximation.
- [44] S. Ciuchi, J. Lorenzana, C. Pierleoni Phys. Rev. B **62**, 4426 (2000).
- [45] N. D. Mermin, Phys. Rev. **176**, 250 (1968).
- [46] L. Bonsall, A. A. Maradudin, Phys. Rev. B **15**, 1959 (1977).
- [47] R. A. Coldwell-Horsfall, A. A. Maradudin, J. of Mathematical Physics **1**, 395 (1960).
- [48] R. E. Peierls, Helv. Phys. Acta **7** (suppl.2) 81 (1936). (see also *Quantum theory of solids* (par 3.3), Oxford University Press (1955)).
- [49] L. D. Landau, E. M. Lifshitz, *Statistical physics*, Pergamon Press N. Y. (1968).
- [50] M. Baus, J. of Statistical Physics **22**, n.1 (1980).
- [51] A. Alastuey B. Jancovici, J. of Statistical Physics **24**, n.3 (1981).
- [52] R. S. Crandall, Phys. Rev. A **8**, 2136 (1973).
- [53] R. C. Gann, S. Chakravarty G. V. Chester, Phys. Rev. B **20**, 326 (1979).
- [54] W. B. da Costa, N. Studart, Phys. Rev. B **47**, 6356 (1993).
- [55] W. Xiaoguang, F. M. Peeters, J. T. Devreese Phys. Rev. B **32**, R6982 (1985).
- [56] F. M. Peeters, J. T. Devreese Phys. Rev. B **36**, 4442 (1987).
- [57] Notice that  $\ell^2(\tau)$  and  $d(\tau)$  are symmetric function respect to time  $\beta/2$  in the interval  $0 < \tau < \beta$  as  $D_o(\tau)$ .
- [58] E. Y. Andrei, **Two-Dimensional Electron Systems on Helium and other Cryogenic Substrates**, (Kluwer Academic Publ. 1997), pags.245-279 and refs. therein.
- [59] E. Y. Andrei, Phys. Rev. Lett. **52**, 1449 (1984).
- [60] C. C. Grimes, G. Adams, Phys. Rev. Lett. **42**, 795 (1979).
- [61] D. S. Fisher, B. I. Halperin, P. M. Platzman, Phys. Rev. Lett. **42**, 798 (1979).
- [62] S. N. Klimin, V. M. Fomin J. Tempere, I. F. Silvera, J. T. Devreese, Sol. Stat. Comm. **126**, 409 (2003).  
J. Tempere, S. N. Klimin, I. F. Silvera J. T. Devreese, Eur. Phys. J. B **32**, 329 (2003).
- [63] V. M. Fomin, M. A. Smondyrev, Phys. Rev. B **49**, 12748 (1994), N. Mori, T. Ando, Phys. Rev. B **40**, 6175 (1989).
- [64] S. A. Jackson, P. M. Platzman, Phys. Rev. B **24**, R499 (1981), S. A. Jackson, P. M. Platzman, Phys. Rev. B **25**, 4886 (1982), M H. Degani, O. Hipolito, Phys. Rev. B **32**, 3300 (1985).